TRAF6 prevents fatal inflammation by homeostatic suppression of MALT1 protease

Authors: Thomas J. O'Neill[1,†], Thomas Seeholzer[1,†], Andreas Gewies[1,†], Torben Gehring[1], Florian Giesert[2], Isabel Hamp[3,4], Carina Graß[1], Henrik Schmidt[5], Katharina Kriegsmann[6], Marie J. Tofaute[1], Katrin Demski[1], Tanja Poth[7], Marc Rosenbaum[8,9], Theresa Schnalzger[8,9], Jürgen Ruland[8,9,10], Martin Göttlicher[11], Mark Kriegsmann[13], Ronald Naumann[14], Vigo Heissmeyer[5,15], Oliver Plettenburg[3,4], Wolfgang Wurst[2,16,17], and Daniel Krappmann[1,*]

Affiliations:
1 Research Unit Cellular Signal Integration, Institute of Molecular Toxicology and Pharmacology, Helmholtz Zentrum München - German Research Center for Environmental Health, 85764 Neuherberg, Germany
2 Institute for Developmental Genetics, Helmholtz Zentrum München - German Research Center for Environmental Health, 85764 Neuherberg, Germany
3 Institute for Medicinal Chemistry, Helmholtz Zentrum München - German Research Center for Environmental Health, 30167 Hannover, Germany
4 Centre of Biomolecular Drug Research (BMWZ), Institute of Organic Chemistry, Leibniz Universität Hannover, 30167 Hannover, Germany
5 Institute for Immunology, Biomedical Center Munich, LMU Munich, 82152 Martinsried, Germany.
6 Department of Hematology, Oncology and Rheumatology, University Hospital Heidelberg, 69120 Heidelberg, Germany
7 Center for Model System and Comparative Pathology (CMCP), Institute of Pathology, University Hospital Heidelberg, 69120 Heidelberg, Germany.
8 Institute of Clinical Chemistry and Pathobiochemistry, TUM School of Medicine, Technical University of Munich, 81675 Munich, Germany.
9 TranslaTUM, Center for Translational Cancer Research, Technical University of Munich, 81675 Munich, Germany.
10 German Cancer Consortium (DKTK), 69120 Heidelberg, Germany
11 Institute of Molecular Toxicology and Pharmacology, Helmholtz Zentrum München - German Research Center for Environmental Health, 85764 Neuherberg, Germany
12 Technical University of Munich, Germany, School of Medicine
13 Institute of Pathology, University Hospital Heidelberg, 69120 Heidelberg, Germany.
14 Max Planck Institute of Molecular Cell Biology and Genetics, Transgenic Core Facility, 01307 Dresden, Germany
15 Research Unit Molecular Immune Regulation, Helmholtz Zentrum München—German Research Center for Environmental Health, 81377 München, Germany
16 German Center for Neurodegenerative Diseases (DZNE), Site Munich, Munich Cluster for Systems Neurology (SyNergy), Munich, Germany
17 Technische Universität München, Lehrstuhl für Entwicklungsgenetik c/o Helmholtz Zentrum München, 85764 Neuherberg, Germany

* Corresponding Author:
Daniel Krappmann
Phone: 0049-89-3187 3461
daniel.krappmann@helmholtz.muenchen.de
† These authors contributed equally to this work

One Sentence Summary:

TRAF6 maintains immune homeostasis by preventing deregulated activation of the MALT1 paracaspase in T cells.

Abstract:

Balanced control of T cell signaling is critical for adaptive immunity and protection from autoimmunity. By combining genetically engineered mouse models, biochemical analyses and pharmacological interventions, we describe an unexpected dual role of the TRAF6 E3 ligase as both a positive and negative regulator of MALT1 paracaspase. While MALT1-TRAF6 recruitment is indispensable for NF-κB signaling in activated T cells, TRAF6 counteracts basal MALT1 protease activity in resting T cells. In mice, loss of TRAF6-mediated homeostatic suppression of MALT1 protease leads to severe autoimmune inflammation, which is completely reverted by genetic or therapeutic inactivation of MALT1 protease function. Thus, TRAF6 functions as a molecular brake for MALT1 protease in resting T cells and a signaling accelerator for MALT1 scaffolding in activated T cells, revealing that TRAF6 controls T cell activation in a switch-like manner. Our findings have important implications for development and treatment of autoimmune diseases.

Introduction

Antigen recognition by T and B cell antigen receptors (TCR/BCR) on lymphocytes initiates adaptive immunity. Upon TCR/CD28 co-ligation on T cells, formation of the higher order CBM complex, consisting of the core subunits CARD11 (CARMA1), BCL10, and MALT1, bridges TCR proximal signaling to the IKK (IκB kinase)/NF-κB and JNK pathways. Within the CBM signaling complex, MALT1 paracaspase exerts a non-catalytic and catalytic function (*1, 2*). MALT1 scaffolding is required to recruit the E3 ligase TRAF6 to the CBM complex, which triggers activation of canonical NF-κB signaling (*3-5*). In parallel, MALT1 protease activity catalyzes the cleavage of substrates involved in cell signaling (e.g. A20, BCL10, CYLD and HOIL-1), transcriptional regulation (RelB) and RNA metabolism (Roquin-1/2, Regnase-1 and N4BP1) (*6-13*).

MALT1 ablation in mice leads to immune deficiency by preventing effective adaptive immune responses (*14, 15*). In contrast, *Malt1* paracaspase mutant (PM) mice, which have defective MALT1 proteolytic activity but retain scaffolding function, develop autoimmune inflammation (*16-20*). Autoimmunity in *Malt1* PM mice has been attributed to developmental loss and functional defects of regulatory T (Treg) cells, which are unable to suppress activation of conventional T (Tconv) effector cells (*19, 21*). Thus, MALT1 protease activity in Treg cells is critical for maintaining immune homeostasis.

The E3 ligase TRAF6 acts as a positive and negative regulator in immune cell signaling (*22*). T cell-specific ablation of TRAF6 in *Traf6*-ΔT mice causes spontaneous T cell activation leading to multi-organ inflammation (*23*). Treg cells are present in *Traf6*-ΔT mice, but the Tconv effector cells escape their suppressive activity, revealing that TRAF6 acts as a T cell-intrinsic negative regulator critical for maintaining immune homeostasis. In Jurkat T cells, TRAF6 is recruited to the CBM complex via distinct TRAF6-binding motifs (T6BM) in MALT1, triggering MALT1 poly-ubiquitination and IKK/NF-κB signaling (*4, 5, 24*). Two alternative MALT1 splice variants exist and while MALT1A encodes two T6BMs, the shorter isoform MALT1B, which lacks exon7, contains only the C-terminal T6BM2 (*3*). *In vitro* experiments in human Jurkat T cells and primary murine CD4+ T cells showed that both T6BMs on MALT1 are essential to channel TCR-induced CBM signaling to NF-κB activation

(*3, 5, 24, 25*). However, the physiological relevance of TRAF6 recruitment to MALT1 for T cell activation or immune homeostasis remained elusive.

To unravel the *in vivo* role of MALT1-TRAF6 binding, we generated *Malt1* TRAF6 binding mutant (TBM) mice by introducing missense mutations in the two T6BMs, rendering MALT1 incapable of interacting with TRAF6. Unexpectedly, loss of MALT1-TRAF6 binding causes constitutive MALT1 protease activation in T cells and provokes a fatal auto-inflammatory disease, which is completely reverted by inactivation of MALT1 paracaspase using CRISPR/Cas9 gene editing in zygotes of *Malt1* TBM mice. Further, disrupted immune homeostasis by conditional T cell-specific TRAF6-deletion in *Traf6*-ΔT mice is ameliorated by treatment with a highly potent MALT1 inhibitor. Thus, our data reveal an unexpected function of TRAF6 in counteracting MALT1 protease activity in resting T cells, which is critical to maintain peripheral immune tolerance.

Results

MALT1-TRAF6 interaction protects from lethal auto-inflammation

Combined mutation of T6BM1 and 2 in MALT1 abolishes TRAF6 association (*3, 24, 25*). We used CRISPR/Cas9 editing to introduce missense mutations in the *Malt1* gene in murine embryonic stem (ES) cells yielding *Malt1* TRAF6 binding mutant (TBM) mice with loss-of-function mutations in T6BM1/2 of MALT1A (E325A;E814A) and T6BM2 of MALT1B (E803A) (**Fig. 1A; Fig. S1A-C**). ES cells containing homozygous alterations in both T6BMs were injected into embryos of C57BL/6 mice. Chimeric offspring were crossed with C57BL/6 mice to obtain heterozygous *MALT1*$^{TBM/+}$ mice, which were further crossed for homozygous *Malt1*$^{TBM/TBM}$ (*Malt1* TBM) mice. Differential PCR and genomic and cDNA sequencing of *Malt1* WT and TBM alleles verified correct genome editing and Western blots showed equivalent protein expression of MALT1 in T cells of *Malt1*$^{+/+}$, *Malt1*$^{TBM/+}$ and *Malt1*$^{TBM/TBM}$ (**Fig. 1B, C; Fig. S1C, D**).

Heterozygous intercrosses yielded homozygous *Malt1* TBM mice at Mendelian ratio. *Malt1* TBM mice stopped thriving between 3 to 4 weeks of age, showed a hunched posture and had to be euthanized

between 3-6 weeks after birth at a median age of 27 days (**Fig. 1D**). Histological analyses of organs showed infiltration of inflammatory cells in the lung, liver, intestines and kidney of moribund mice (**Fig. 1E**). *Malt1*$^{TBM/TBM}$ mice were analyzed at day 18, before they displayed severe burden or significant weight loss, and were compared to heterozygous *Malt1*$^{TBM/+}$ which appeared normal at this age (**Fig. 1F**). Splenomegaly and lymphadenopathy were observed in *Malt1* TBM mice (**Fig. 1G**). In line with multi-organ inflammation, the cytokines TNFα, IFNγ, IL-6, IL-10 and IL-17 were upregulated in sera of *Malt1* TBM mice (**Fig. 1H**). The observed phenotype was persistent through 6 generations of *Malt1* TBM backcross to C57BL/6 mice. Thus, mice with homozygous TBM mutations and consequent loss of MALT1-TRAF6 interaction develop a fatal inflammatory pathology.

Immune phenotyping at day 18 after birth revealed that total numbers of splenic B220+ B cells were markedly decreased, while T cells numbers remained similar (**Fig. 2A, B; Fig. S2A, B**). This resulted in a relative increase of CD3+, CD4+ and CD8+ T cells in the spleen but not lymph nodes in *Malt1* TBM mice (**Fig. 2C; Fig. S2C**). T cell subsets in the thymus were normal, indicating no obvious developmental defects (**Fig. S2D, E**). Relative B220+ B cell numbers in the spleen and lymph nodes were reduced, but not in bone marrow (**Fig. 2D**). T cells from *Malt1* TBM mice displayed high expression of CD69, and B cells exhibited high levels of CD69 and CD86, indicating lymphocyte activation (**Fig. S3A-F**). Inspection of T cells demonstrated a massive accumulation of CD44^{hi}CD62L^{lo} CD4+ and CD8+ effector/memory T cells (T_{EM}) and a concomitant decrease of naive CD44^{lo}CD62L^{hi} CD4+ and CD8+ T cells (T_{naive}) in spleen and lymph nodes of *Malt1* TBM mice (**Fig. 2E-J; Fig. S3G, H**). The autoimmune pathology upon defective protease activity in *Malt1* PM mice has been attributed to a strong decrease in Treg cell numbers and function (*16-19, 21*). In contrast, numbers of CD4+FoxP3+ Treg cells and CD44^{hi}CD62L^{lo} CD4+ effector (e)Treg cells were increased in *Malt1* TBM mice compared to heterozygous littermates (**Fig. 2K-M**). eTreg cells from *Malt1* TBM homo- and heterozygous mice expressed equivalent or higher levels of the suppression markers CTLA-4 or OX40, respectively (**Fig. 2N; Fig. S3I, J**). Thus, loss of TRAF6 binding to MALT1 leads to spontaneous lymphocyte activation and a severe immune pathology, which is not accompanied by a loss of Treg cells as observed upon mutation of the MALT1 catalytic site (*16, 18, 19*).

Heterozygous *Malt1*$^{TBM/+}$ mice were phenotypically normal at three months after birth, and up to one year of age they did not display weight loss or obvious disease symptoms compared to *Malt1*$^{+/+}$ littermates (**Fig. S3K**). However, heterozygous animals exhibited splenomegaly accompanied by an increase in the CD4+ and CD8+ T_{EM} cell populations at 6 months and even more pronounced at 12 months of age (**Fig. 2O, P**). As observed in young homozygous *Malt1*$^{TBM/TBM}$ mice, the number of CD4+FoxP3+ Treg cells were increased in aged *Malt1*$^{TBM/+}$ mice (**Fig. S3L**). Thus, MALT1 TBM protein causes immune activation even in the presence of MALT1 WT, but the milder and delayed onset of the phenotype indicates that MALT1 WT may act in a dominant manner.

Binding of MALT1 to TRAF6 is critical for T cell homeostasis

Since MALT1 is critical for functional responses of conventional and regulatory T cells, we wanted to investigate the T cell-intrinsic role of MALT1-TRAF6 interaction in the maintenance of immune homeostasis. We generated *Malt1*$^{TBM/fl}$*;CD4-Cre* (*Malt1 TBM-T*) mice, which have conditional deletion of the floxed *Malt1* WT allele in CD4+ and CD8+ T cells. MALT1 TBM protein expression was normal in CD4+ T cells from *Malt1*$^{TBM/fl}$*;CD4-Cre* mice (**Fig. 3A**). *Malt1* TBM-T mice were viable, but like *Traf6*-ΔT mice (*23*), they developed skin eczema and epidermal inflammation beyond 12 weeks of age, showing a T cell-driven immune disorder (**Fig. 3B; Fig. S4A**). We bred *Traf6*$^{fl/fl}$*;CD4-Cre* (*Traf6*-ΔT) mice, which lack TRAF6 expression in CD4+ and CD8+ T cells (**Fig. 3C**), to directly compare phenotypes caused by complete loss of TRAF6 and destruction of MALT1-TRAF6 binding in T cells. In addition, we assessed the effects of MALT1 TBM expression solely in Treg cells, by crossing *Malt1*$^{TBM/fl}$ and *FoxP3-Cre* (*Malt1* TBM-Treg). *Malt1* TBM-Treg mice did not show any symptoms or signs of disease up to 15 weeks of age.

At 12 weeks of age, *Malt1* TBM-T, *Traf6*-ΔT and *Malt1* TBM-Treg mice exhibited no weight loss, but enlarged spleens were observed in *Malt1* TBM-T and *Traf6*-ΔT, but not in *Malt1* TBM-Treg mice (**Fig. 3D; Fig. S4B**). No significant changes in relative CD3+ T or B220+ B cell numbers were observed in the three genotypes (**Fig. S4C, D**). Relative numbers of CD4+ T cells were slightly elevated in *Malt1*

TBM-T mice, whereas CD8+ T cells were decreased in *Malt1* TBM-T and *Traf6*-ΔT mice (**Fig. 3E, F**). As evident from an increase in CD69-expressing CD3+ T cells as well as expansion of the $CD44^{hi}CD62L^{lo}$ CD4+ and CD8+ T_{EM} populations, T cells become similarly activated by a cell-intrinsic mechanism upon MALT1 TBM expression or TRAF6 ablation (**Fig. 3G-L; Fig. S4E**). No changes in the relative numbers of T_{EM}, T_{CM} and T_{naive} cells were detected in *Malt1* TBM-Treg mice, revealing that T cell activation is not caused by functional inactivation of Treg cells. Numbers of CD4+FoxP3+ Treg cells were even increased in *Malt1* TBM-T mice and slightly elevated in *Malt1* TBM-Treg mice (**Fig. 3M**). While Treg cell numbers were normal in *Traf6*-ΔT mice, eTreg cells and expression of suppression marker OX40 were higher in mice from all three genotypes (**Fig. 3N, O**). *In vitro* Treg cells from *Malt1* TBM-T mice suppressed proliferation of CD4+ T cells, revealing that they retain their suppressive function (**Fig. S4F, G**). Expression of CD69 and CD86 activation markers on B220+ B cells was increased in mice carrying T cell-specific *Malt1* TBM-T or *Traf6*-ΔT gene alterations (**Fig. 3P, Q**), but the effect was less pronounced compared to *Malt1* TBM mice (see **Fig. S3**). Nevertheless, B cell activation led to elevated anti-dsDNA autoantibodies in sera of *Malt1* TBM-T and *Traf6*-ΔT mice (**Fig. 3R**). Thus, destruction of MALT1-TRAF6 interaction or deletion of TRAF6 in T cells provokes a highly similar, cell-intrinsic hyper-activation of Tconv effector cells and ultimately autoimmunity. The lack of any signs of T cell activation in *Malt1* TBM-Treg mice indicates that autoimmune inflammation upon loss of MALT1-TRAF6 binding is not caused by disrupted Treg development or function.

MALT1-TRAF6 drives TCR-induced NF-κB and antagonizes basal MALT1 protease activity

To investigate the cause of T cell activation upon loss or MALT1-TRAF6 binding, we analyzed NF-κB activation in CD4+ T cells isolated from *Malt1* TBM-T and *Traf6*-ΔT mice after αCD3/CD28 or PMA/Ionomycin (P/I) stimulation. Induction of IκBα phosphorylation and degradation, p65 phosphorylation and NF-κB DNA binding was strongly impaired in *Malt1* TBM-T as well as *Traf6*-ΔT CD4+ T cells (**Fig. 4A, B; Fig. S5A, B**). No change was observed in constitutive or inducible AKT phosphorylation in T cells from *Malt1* TBM-T or *Traf6*-ΔT mice (**Fig. S5A, B**). We performed

quantitative flow cytometric imaging analyses of NF-κB nuclear translocation in CD4+ T cells. While P/I stimulation prompted nuclear translocation of the canonical NF-κB subunits p65 and c-Rel in WT CD4+ T cells, translocation was strongly impaired in CD4+ T cells from *Malt1* TBM-T and *Traf6*-ΔT (**Fig. 4C-F; Fig. S5C-F**). Thus, we demonstrate that TCR-induced activation of canonical NF-κB signaling relies on the presence of TRAF6 and its interaction with MALT1 in murine CD4+ T cells.

Surprisingly, we consistently noticed augmented cleavage of MALT1 substrates CYLD and Regnase-1 even in the absence of T cell stimulation in CD4+ T cells from *Malt1* TBM-T and *Traf6*-ΔT mice, indicating constitutive MALT1 protease activation upon loss of TRAF6 expression or destruction of MALT1-TRAF6 interaction (**Fig. 4A, B; Fig. S5A, B**). Yet, constitutive MALT1 substrate cleavage was increased upon P/I or αCD3/CD28 stimulation. To confirm spontaneous MALT1 protease activation, we analyzed MALT1 substrates in CD4+ T cells isolated from a panel of *Malt1* TBM-T and *Traf6*-ΔT mice and constitutive cleavage of CYLD, HOIL-1, Regnase-1 and Roquin-1/2 was detected in all samples when compared to controls (**Fig. 4G, H**). To determine functional consequences, we analyzed expression of NFKBID/IκBNS and ICOS in *Malt1* TBM-T and *Traf6*-ΔT CD4+ T cells, which are tightly controlled by the post-transcriptional regulators and MALT1 substrates Regnase-1 and Roquin-1/2 (*12, 18, 26, 27*). Furthermore, the potent and selective MALT1 protease inhibitor MLT-943 suppressed TCR/CD28-induced upregulation of IκBNS and ICOS on murine CD4+ T cells, confirming their tight regulation by MALT1 (**Fig. S5G**) (*28, 29*). In agreement with augmented cleavage of Regnase-1 and Roquin-1/2, IκBNS and ICOS expression were upregulated in CD4+ and CD8+ T cells from *Malt1* TBM-T and *Traf6*-ΔT mice (**Fig. 4I, J; Fig. S5H**). Thus, our data provide evidence that despite defective NF-κB signaling, complete loss of TRAF6 or selective loss of MALT1-TRAF6 interaction leads to deregulated basal MALT1 protease activation in T cells, which is sufficient to partially inactivate post-transcriptional control mechanisms by the RNA binding proteins (RBPs) Regnase-1 and Roquin-1/2.

TRAF6 counteracts constitutive MALT1 protease activity in resting T cells

Due to increased T_{EM} cell population, it is difficult to dissect the cellular mechanism and origin of constitutive MALT1 protease activity in CD4+ T cells taken from *Malt1* TBM-T and *Traf6*-ΔT mice. To address the T cell-intrinsic impact of TRAF6 on MALT1 protease activity in the absence of secondary effects caused by the autoimmune/inflammatory phenotype, we switched to a heterologous system. We transduced MALT1 KO Jurkat T cells with MALT1A and MALT1B WT and the respective TRAF6 binding mutants (human MALT1A E316A/E806A and MALT1B E795A) (**Fig. 6SA, B**). MALT1A E316A/E806A and MALT1B E795A failed to rescue IκBα degradation and thus NF-κB activation after P/I stimulation. As observed in *Malt1* TBM-T CD4+ T cells, constitutive cleavage of MALT1 substrates CYLD, Regnase-1, Roquin-1/2 and HOIL-1 was detected in MALT1 KO Jurkat T cells rescued with MALT1A E316A/E806A or MALT1B E795A, but not the respective WT isoforms. We used a biotinylated MALT1 activity-based probe (bio-MALT1-ABP), which covalently binds active MALT1 and allows direct measurement of cellular MALT1 protease activity (*30*). Active MALT1 and cleavage of substrates were detected in resting Jurkat T cells containing the TRAF6 binding mutants MALT1A E316A/E806A or MALT1B E795A, and constitutive protease activity was abolished in the MALT1B active site mutant C453A (**Fig. 5A**). Constitutive and inducible cleavage of CYLD took place at position R324, demonstrating identical substrate selectivity for chronic and inducible MALT1 activity (**Fig. S6C**). We performed *in vitro* MALT1 activity measurements and found that the cleavage rates of a fluorogenic substrate (k_{cat} and K_M values) were similar for recombinant purified GST-MALT1B WT and E795A mutant protein, revealing that the T6BM mutation does not intrinsically affect MALT1 protease activity (**Fig. S6D**).

To learn more about the molecular requirements of constitutive MALT1 protease activation, we determined the consequences of defective BCL10 binding (MALT1B V81R), MALT1 dimerization (MALT1B K513E) or MALT1 mono-ubiquitination (MALT1B K633R) in the context of the TBM MALT1B E795A (*31-33*). Similar to inducible MALT1 protease activation, constitutive cleavage of the MALT1B E795A mutant strictly relied on N-terminal BCL10 interaction, the ability of MALT1 to dimerize through the paracaspase domain and mono-ubiquitination in the C-terminal Ig3 domain (**Fig. 5B; Fig. S6E**). As expected, the single MALT1 dimerization or mono-ubiquitination mutants did not

severely affect NF-κB signaling (*34*). Thus, the same molecular mechanisms control inducible and constitutive MALT1 protease activity in T cells.

We recently identified the human hypomorphic germline MALT1 mutation (c.2418G>C) which leads to the Glu(E) to Asp(D) exchange in the T6BM2 motif (*25*). This missense mutation selectively affects TRAF6 binding and NF-κB activation of the MALT1B isoform, which causes a severe primary immune disorder with signs of immune deficiency and autoimmunity. Indeed, the conserved E795D mutation in MALT1B not only abrogates NF-κB signaling, but also induces constitutive MALT1B activation comparable to the MALT1B E795A exchange, while the same exchange in T6BM2 of MALT1A (E806D) does not affect MALT1A signaling and protease activity in the presence of a functional T6BM1 (**Fig. 5C; Fig. S6F**). To address if MALT1 WT has a dominant effect over the TBM mutant, as suggested by the mild phenotype of heterozygous *Malt1* TBM mice (**Fig. 2O,P**), we simultaneously transduced increasing amounts of MALT1A WT and pathogenic MALT1B E795D (**Fig. 5D**). MALT1A WT neutralized constitutive substrate cleavage by MALT1B E795D in a dominant negative manner and hardly any substrate cleavage was detected at a 1:1 ratio, explaining the mild T_{EM} phenotype in heterozygous *Malt1*$^{TBM/+}$ mice (compare **Fig. 2O, P**). However, MALT1B is the major isoform expressed in peripheral murine and human T cells (*3*), which we also confirmed at the transcript level for CD4+ T cells from *Malt1* TBM-T mice (**Fig. S6G**). Thus, constitutive MALT1 protease activation by the selective destruction of MALT1B T6BM2 appears to be sufficient to drive the primary human immune pathology.

Next, we asked if and how TRAF6 negatively impacts MALT1 protease activity in Jurkat T cells. We generated TRAF6 KO Jurkat T cell clones. TNFα-induced NF-κB activation was normal in the absence of TRAF6, but NF-κB signaling and activation of an NF-κB-EGFP reporter gene after TCR/CD28 or P/I stimulation was abolished in TRAF6 KO Jurkat T cells verifying the essential role of TRAF6 for TCR-induced NF-κB activation (**Fig. 5E; Fig. S7A, B**). While AP-1 activation was mildly impaired, NF-AT activation was unchanged in TRAF6 KO or MALT1B E795A reconstituted Jurkat T cells gene following TCR/CD28 stimulation (**Fig. S7C, D**). Mirroring the results in murine TRAF6-deficient CD4+ T cells, MALT1 protease was constitutively active as evident from augmented MALT1 substrate

cleavage and MALT1-ABP detection even in the absence of T cell stimulating agents (**Fig. 5F, G**). We reconstituted TRAF6 KO Jurkat T cells with TRAF6 WT, the C70A E3 ligase mutant or the R88A/F118A oligomerization mutant (*35*). TRAF6 WT rescued NF-κB signaling and counteracted chronic MALT1 protease activity as seen by diminished MALT1-ABP binding and cleavage of CYLD, Regnase-1 and HOIL-1 in the absence of stimulation (**Fig. 5H**). Neither TRAF6 C70A nor TRAF6 R88A/F118A could compensate for the loss or TRAF6, demonstrating that TRAF6 E3 ligase activity and self-assembly is required to promote NF-κB signaling and to retain MALT1 protease inactive in resting T cells (**Fig. 5H; Fig. S7E**).

To understand the cellular cause of constitutive MALT1 activity in the absence of TRAF6, we wanted to test the requirement of upstream signaling components for constitutive MALT1 protease activity in TRAF6 KO Jurkat T cells. We first generated TRAF6/BCL10 and TRAF6/CARD11 double KO Jurkat T cells to address the necessity of CBM complex assembly. In agreement with our previous observation that MALT1 needs to interact with BCL10 (see **Fig. 5B**), constitutive MALT1 substrate cleavage in TRAF6 KO cells was lost in TRAF6/BCL10 KO Jurkat T cells (**Fig. 5I; Fig. S7F**). Further, additional CARD11 deficiency completely abrogated constitutive MALT1 substrate cleavage in the TRAF6 KO Jurkat T cells, indicating that CBM complex formation is necessary for constitutive MALT1 activity (**Fig. 5I; Fig. S7G**). To determine if low levels of cell-autonomous TCR signaling even in the absence of an external trigger causes constitutive MALT1 protease activation, we deleted the TCRα chain in TRAF6 KO Jurkat T cells via CRISPR/Cas9. Ablation of TCRα leads to a collapse of the surface expression of the multi-protein TCR complex, as evident from the absence of CD3ε surface expression in TCRα/TRAF6 dKO Jurkat T cell clones (**Fig. 5J**) (*36*). Indeed, constitutive MALT1 substrate cleavage was lost in TCRα/TRAF6 dKO Jurkat T cells (**Fig. 5K**). As expected, MALT1 protease activity was also no longer stimulated by αCD3/CD28, but loss of TCR signaling could be bypassed by P/I stimulation, demonstrating no general defect in MALT1 protease activation in these cells (**Fig. S7H**). Thus, TRAF6 E3 ligase negatively affects basal MALT1 protease activity by antagonizing low level cell-autonomous TCR signaling in unstimulated T cells.

MALT1 protease drives lethal inflammation upon loss of TRAF6 binding

To prove that constitutive MALT1 protease activation drives lethal inflammation upon loss of TRAF6 binding, we introduced the paracaspase mutation C472A by CRISPR/Cas9 and homology directed repair in *Malt1*$^{TBM/+}$ zygotes. This approach yielded offspring with the correct MALT1 paracaspase mutation (PM) on the same allele as the T6BM1/2 mutations and we ultimately obtained homozygous *Malt1*$^{TBMPM/TBMPM}$ (*Malt1* TBMPM) mice (**Fig. S8A, B**). Genotypes were verified by PCR, restriction digestion and sequencing, and MALT1 TBMPM protein was expressed in splenocytes of *Malt1* TBMPM mice at equivalent levels to controls (**Fig. 6A, B**). Except for one mouse, which died of unknown cause at day 27, *Malt1*$^{TBMPM/TBMPM}$ mice appeared healthy, and no weight loss, enlarged spleens or macroscopic signs of inflammation were observed 8 weeks after birth (**Fig. 6C, D**). Analogous to the situation in *Malt1*$^{-/-}$ mice, scaffold-mediated NF-κB signaling and MALT1 protease activity were lost in CD4+ T cells from *Malt1*$^{TBMPM/TBMPM}$ mice (**Fig. 6E; Fig. S8C, D**). Overall lymphocyte frequencies were not severely affected in *Malt1* TBMPM animals (**Fig. S8E-H**). As observed in *Malt1*$^{-/-}$ mice, *Malt1*$^{TBMPM/TBMPM}$ mice are nearly devoid of peripheral and thymic Treg cells and peritoneal B1 B cells (**Fig. 6F, G; Fig. S8I, J**). Contrary to immune activation observed in *Malt1* TBM and *Malt1* PM mutant mice (compare **Fig. 2; Fig. 3**) (*16-19*), lymphocyte activation markers CD69 and CD86 were reduced and we observed a decrease in CD44^{hi}CD62L^{lo} T_{EM} cells in *Malt1*$^{TBMPM/TBMPM}$ mice compared to heterozygous littermate controls (**Fig. 6H; Fig. S8K-N**). As seen in *Malt1*$^{-/-}$ mice, serum concentrations of IFNγ and TNFα cytokines remained low in *Malt1*$^{TBMPM/TBMPM}$ mice (**Fig. 6I; Fig. S8O**). Thus, the fatal auto-inflammation triggered by the selective destruction of MALT1-TRAF6 interaction is driven by constitutive MALT1 protease activity. Conversely, autoimmune activation in MALT1 paracaspase inactive mice relies on MALT1-TRAF6 binding and MALT1 scaffolding.

MALT1 inhibitor treatment restores T effector cell homeostasis upon loss of TRAF6

We asked if pharmacologic inhibition of constitutive MALT1 protease activation is able to ameliorate uncontrolled immune activation resulting from T cell specific TRAF6 ablation. We evaluated inhibition

of constitutive MALT1 protease activity by MLT-943 and MLT-985, two potent MALT1 inhibitors (*28, 37*). In line with previous reports, MLT-985 was slightly more potent (2-3 fold) than MLT-943 in inhibiting constitutive MALT1 protease activity in TRAF6 KO Jurkat T cells (**Fig. 7A**) (*37*). Compared to MLT-943, MLT-985 displayed superior pharmacokinetics and improved bioavailability in mice (*37*) and therefore was chosen to achieve effective inhibition of chronic MALT1 activity *in vivo*. We started a therapeutic regime with treatment of *Traf6*-ΔT mice with MLT-985 at 8 weeks of age after the onset of T cell hyper-activation (*23*). MLT-985 was administered at 16 mg/kg (intraperitoneal, bi-daily) for 10 consecutive days to achieve optimal MALT1 inhibition throughout the treatment (**Fig. 7B**). At the end of the treatment period, splenic CD4+ T cells were isolated and Western blot demonstrated that MLT-985 treatment effectively abolished constitutive MALT1 substrate cleavage in *Traf6*-ΔT mice when compared to vehicle control (**Fig. 7C**). Further, MALT1 protease-dependent upregulation of IκBNS and ICOS was reduced by the MLT-985 treatment to the expression levels observed in WT mice (**Fig. 7D**). Immune phenotyping demonstrated that concomitant T cell activation was ameliorated in *Traf6*-ΔT mice after 10 days of MALT1 inhibitor treatment, as reflected by reduced surface expression of CD69 on T cells and a strong decrease in relative numbers of T_{EM} cells (**Fig. 7E, F**). Expression of T cell activation markers were reduced to levels detected in WT mice. Despite the therapeutic improvements of autoimmune symptoms, MLT-985 treatment resulted in a severe reduction in the frequency of splenic CD4+FoxP3+ Treg cells in *Traf6*-ΔT mice (**Fig. 7G**), which confirms previous observations on decreased Treg cells after *in vivo* application of potent MALT1 inhibitors (*28, 38*). Additionally, the Treg cell suppression marker OX40 was decreased in response to MLT-985 (**Fig. 7H**). Importantly, notwithstanding the loss of Treg cells, T cell hyper-activation in *Traf6*-ΔT mice is completely reverted by MALT1 inhibition, providing evidence that loss of TRAF6 drives autoimmune inflammation by unopposed MALT1 protease activity in Tconv effector cells.

Discussion

Our findings provide the explanation for the long-standing paradox how TRAF6 can exert its dual T cell-intrinsic functions and act at the same time as a positive regulator of immune activation and as a negative factor for maintenance of immune homeostasis. We demonstrate that both positive and negative functions of TRAF6 strictly rely on its ability to interact with MALT1. In line with previous *in vitro* data (*3, 5, 24*), TRAF6 binding to MALT1 within the assembled CBM signaling complex mediates activation of canonical IKK/NF-κB signaling *in vivo*. Simultaneously, selective destruction of the TRAF6 interaction interface on MALT1 or complete loss of TRAF6 renders MALT1 protease constitutively active, leading to the unexpected identification of TRAF6 as an essential negative regulator of the MALT1 protease in resting T cells. Thus, destruction of MALT1-TRAF6 interaction provokes a loss-of function in the context of NF-κB activation, and a gain-of-function leading to constitutive MALT1 protease activation. We show that the lethal auto-inflammation upon loss of MALT1-TRAF6 interaction is caused by the gain of MALT1 proteolytic activity, because it is fully reverted by the catalytically inactive MALT1 paracaspase mutation (PM). Moreover, therapeutic MALT1 inhibitor treatment improves autoimmune/inflammatory symptoms caused by ablation of TRAF6, proving that the gain in MALT1 protease activity is also responsible for T cell activation and autoimmunity in the absence of TRAF6.

To obtain mechanistic insights, we used Jurkat T cell as a heterologous model system for TCR signaling to study cell-autonomous effects of TRAF6 ablation on MALT1 protease activity independent of the auto-inflammatory milieu. In Jurkat T cells, expression of MALT1 T6BM mutants or TRAF6-deficiency fully recapitulates the augmented MALT1 protease activation seen in *Malt1* TBM-T and *Traf6*-ΔT mice. The autoimmune and inflammatory environment represents an experimental caveat for the biochemical analyses of murine CD4 T cells isolated from *Malt1* TBM mice and we cannot exclude that MALT1 protease activation is further boosted by extracellular factors *in vivo*. Nevertheless, the heterologous Jurkat system provides strong evidence that constitutive MALT1 protease activation in the absence of TRAF6 expression or interaction is not primarily resulting from the inflammatory environment, but that TRAF6 functions as a cell-intrinsic negative regulator of the MALT1 protease in resting T cells. Our dissection of the molecular mechanisms revealed that identical pathways are

operational for constitutive and TCR-induced MALT1 protease activation. On the side of MALT1, these include the necessity for mono-ubiquitination, dimerization of the paracaspase domain and BCL10 association (*31-33*).

Since CARD11-deficiency, and thus the inability to form a functional CBM complex, abolished constitutive MALT1 protease activity in TRAF6 KO Jurkat T cells, we hypothesized that TRAF6 might prevent MALT1 protease activation arising from cell-autonomous low level TCR signaling in the absence of a high-affinity antigen-ligand. Indeed, destruction of the TCR multi-protein complex by a TCRα KO completely prevented constitutive MALT1 substrate cleavage in TRAF6 KO Jurkat T cells. Thus, TRAF6 E3 ligase activity counteracts homeostatic TCR signaling to prevent low levels of CBM complex activation in T cells in the absence of a strong antigenic challenge. At present it is unclear whether constitutive MALT1 protease activation *in vivo* is caused by cell-autonomous TCR assembly, or by tonic T cell signaling through transient interactions of the TCR with self-peptide-MHCs in the periphery (*39*). However, homeostatic suppression of MALT1 protease by TRAF6 is essential for maintaining the inhibitory tone on naive T cells that prevents hyper-activation. Since MALT1-TRAF6 interaction drives NF-κB downstream signaling upon T cell activation, our analyses define this interaction as a critical control switch that balances T cell homeostasis and activation in the regulation of adaptive immune responses. Our mechanistic analyses rely on specific loss-of-function mutations, which abolish critical protein-protein interactions or enzymatic activities. The data provide indirect evidence that TRAF6 E3 ligase activity counteracts CBM formation upon binding to MALT1 under steady state conditions. However, we lack sensitive biochemical tools to demonstrate directly MALT1-TRAF6 association, CBM complex formation or substrate ubiquitination in the absence of antigenic stimulation. Thus, measuring these low level and most likely transient interactions and modifications represents an experimental limitation of this study.

Even though constitutive MALT1 protease activation represents a gain-of-function, which is induced by the TBM mutations, heterozygous *Malt1*$^{TBM/+}$ mice only develop a mild immune activation phenotype with a delayed onset. We demonstrate that expression of MALT1A WT limits protease activity of MALT1B E795D mutant in a dominant manner. Dimerization of MALT1 TBM is required

for constitutive MALT1 protease activity and CARD11-BCL10 may even induce further clustering of MALT1. Thus, in the presence of the MALT1 WT protein, TRAF6 recruitment to the CBM complex is not completely abolished and can still interrupt cell-autonomous TCR-dependent MALT1 protease activation in a dominant-negative manner. Importantly, MALT1B lacks T6BM1 in exon7 and is the major isoform expressed in peripheral murine and human T cells (*3*). Selective destruction of the MALT1 T6BM2 is sufficient to drive a severe primary immune disorder in a human patient (*25*) and our data suggest that MALT1B protease is constitutively active, because MALT1A is not present to counteract MALT1B activity in a dominant-negative manner.

TRAF6 deficiency promotes constitutive MALT1 protease activation but impairs MALT1 scaffolding and TCR-induced NF-κB activation, posing the question how deregulated MALT1 protease activity drives autoimmune inflammation. Continuous MALT1 substrate cleavage even in the absence of TCR-induced NF-κB is sufficient to trigger autoimmune inflammation. This suggests a crucial role on the level of post-transcriptional gene regulation, because the MALT1 RBP substrates Regnase-1 and Roquin-1/2 are critical for maintenance of peripheral tolerance (*11, 12, 40-42*). Interestingly, T cell-specific deletion of Regnase-1 or the combined ablation of Roquin-1 and Roquin-2 paralogs triggers autoimmune inflammation, also characterized by a cell-autonomous increase in effector memory T cells (*12, 42, 43*). In fact, *Malt1* TBM-T and *Traf6*-ΔT mice display a similar but milder phenotype compared to conditional Regnase-1 or Roquin-1/2 ablation in T cells. In line, expression of ICOS, NFKBID/IκBNS and OX40, which are suppressed by Regnase-1 and/or Roquin1/2 (*12, 42*), is upregulated in T cells from *Malt1* TBM-T and *Traf6*-ΔT mice. Thus, our results suggest that constitutive MALT1 protease activity drives aberrant immune activation of Tconv cells by deregulated cleavage and partial inactivation of these critical post-transcriptional regulators.

Strikingly, either permanent inactivation or chronic activation of MALT1 protease provokes autoimmunity and inflammation, but both diseases are driven by very distinct cellular and molecular mechanisms. Defective MALT1 paracaspase activity in *Malt1* PM mice leads to autoimmunity resulting from impaired Treg cell development and function (*17, 19*). In contrast, *Malt1* TBM Treg cells are functional in *in vitro* suppression assays and Treg cell numbers and expression of suppression markers

are not decreased in *Malt1* TBM mice displaying constitutive MALT1 protease activity. Moreover, while mice with Treg-selective ablation of CBM subunits or MALT1 protease inactivation develop severe autoimmune inflammation (*21, 44*), Treg-restricted loss of MALT1-TRAF6 binding does not lead to any discernible immune phenotype. In fact, TRAF6-deficient Tconv effector cells have become insensitive to suppression by Treg cells (*23*). Further, we demonstrate that pharmacological MALT1 inhibition decreases the numbers of FoxP3+CD4+ Treg cells and expression of OX40 in *Traf6*-ΔT mice, but still silences Tconv cell activation and generation of T_{EM} cells. Our results underscore that the changes in Tconv cells, and not Treg cells, are responsible for the severe immune imbalance caused by TRAF6 ablation or loss of MALT1-TRAF6 interaction. The strong activation of T_{EM} cells in *Malt1* TBM mice may limit the ability to detect more subtle changes in the suppressive functions of Treg cells, which may still at least partially contribute to the immune pathology.

We demonstrate that faithful homeostasis and activation in the adaptive immune system relies on the intricate balance of MALT1 scaffolding and protease function. MALT1 protease inactivation rescues the disease triggered by loss of MALT1-TRAF6 binding and, vice versa, autoimmune inflammation caused by MALT1 protease inactivation strictly relies on TRAF6 recruitment. Thus, while *Malt1* TBM drives inflammation independent of downstream NF-κB activation, MALT1/TRAF6-dependent NF-κB signaling is required to drive autoimmunity in protease-inactive *Malt1* PM mice. The *Malt1* TBMPM mice provide unequivocal proof that MALT1 scaffolding function and NF-κB activation are responsible for the immune imbalance in *Malt1* PM mice (*16, 18, 19*). In fact, *Malt1* TBMPM mice are phenotypically indistinguishable from *Malt1*$^{-/-}$ mice, showing that only the combined defects in protease activity and TRAF6 recruitment prevent autoimmunity and cause immunodeficiency. The milder autoimmune phenotype in conditional *Malt1* TBM-T mice suggests that other cell types such as B cells and myeloid cells are contributing to the fatal inflammation in *Malt1* TBM mice. Peripheral B cell numbers are decreased in *Malt1* TBM mice, which is likely a result and not a cause of auto-inflammation, because similar effects have been reported in other autoimmune-inflammatory models, including the T cell-specific ablation of Roquin1/2 (*42*). B cell numbers in *Malt1* TBM-T mice are unchanged, suggesting that the effect is triggered by a complex interplay of different immune cells.

In summary, by tightly regulating MALT1 scaffold and protease functions, TRAF6 acts in a switch-like manner to balance immune homeostasis and activation. These finding are of high clinical relevance. Recently, we have described a primary human immune disorder with signs of immunodeficiency and autoimmunity, which is linked to a germline *MALT1* mutation that selectively destroys TRAF6 binding to the MALT1B isoform (*25*). We show here that this mutation not only abrogates NF-κB signaling by MALT1B, but also renders MALT1B protease constitutively active, providing evidence that MALT1-TRAF6 interaction is critical for immune homeostasis and activation in humans. Further, genetic variants of *TRAF6* are associated with higher risks for systemic lupus erythematosus and rheumatoid arthritis (*45, 46*). Treatment with a potent MALT1 inhibitor neutralizes T cell hyper-activation by TRAF6 ablation, despite the severe reduction in immunosuppressive Treg cells. Our data suggest that there may be a therapeutic window for the use of MALT1 inhibitors to treat immune diseases linked to disruption of MALT1-TRAF6 association or TRAF6 loss-of-function, but analyses of patient biopsies will be critical to link our findings to human autoimmune/inflammatory pathologies. Further, the decrease in Treg cells upon MALT1 inhibition will certainly pose a limitation to such therapeutic approaches, but Treg cells recover rapidly after inhibitor withdrawal (*28*), indicating that intermittent treatment may be an option for managing acute disease episodes.

Material and Methods

Study design

The aim of this study was to define the physiological role of MALT1-TRAF6 interaction. Several mouse models were generated to abolish MALT1-TRAF6 interaction or to delete TRAF6. To investigate the cell-autonomous role for MALT1-TRAF6 interactions, we used flow cytometry, cytokine analyses, histology and *ex vivo* analyses of T cells signaling (Western blot, imaging). We used primary T cells and in Jurkat T cells to study the effect of TRAF6 ligase activity on MALT1 protease activity in resting T cells. Based on these findings, we designed two experiments to prove that constitutive MALT1 protease activity causes autoimmunity and inflammation: (a) *In vivo* genetic rescue of auto-inflammation in *Malt1* TBM mice by CRISPR/Cas9-triggered mutation of MALT1 protease active site

and (b) amelioration of autoimmunity by pharmacological MALT1 inhibition of *Traf6*-ΔT mice. For mouse studies, statistical design and replications were performed as mandatory for legal approval for animal experimentations. Age-matched littermates with equivalent genetic background were used. Reported phenotypes remained reproducible for at least six generations. Randomization was performed prior to mouse treatment shown in Fig. 7. Investigators were not blinded. Replicates are presented as individual dots in the figures. No data were excluded from analyses. Statistical methods are described in figure legends material and methods.

Mice

All mouse experiments were performed in accordance with the guidelines of the Federation of European Laboratory Animal Science Association (FELASA) and were approved by the Regierung von Oberbayern (Ref. No.: 55.2-2532-VET_02-17-122 and 55.2-2532.Vet_02-19-112).

Generation of *Malt1* TBM strain

Malt1 TBM (TBM: TRAF6 binding mutant) mice carrying genomic missense mutations in TRAF6 binding motif 1 and 2 (T6BM1 and 2) were generated by CRISPR/Cas9 mutagenesis in R1/E (129S1/X1) ES cells and embryo injection. *Malt1* TBM mice express the mutant variants MALT1A E325A;E814A and MALT1B E803A. For mutagenesis of the two TRAF6 binding motifs (T6BMs) in MALT1 (T6BM1 in exon 7 and T6BM2 in exon 17) targeting sequences for single guide (sg) RNAs were designed using the GPP sgRNA Designer provided by the BROAD Institute (*55*) (https://portals.broadinstitute.org/gpp/public/analysis-tools/sgrna-design). The respective coding DNA sequences were cloned into pX458 plasmid (Addgene #48138). Short single stranded oligodeoxyribonucleotides (ssODNs) homology directed repair (HDR) templates were synthesized that introduce TRAF6 binding mutation 1 and 2 (TBM1 and TBM2) and alterations in the PAM sequences by silent mutations to prevent multiple Cas9 cleavage events at the locus in the *Malt1* gene. Additional silent mutations in the region of the TBM mutations were inserted to enable differential PCR amplification by WT- and mutation-specific PCR primers for the identification of targeted alleles in ES cell clones and genotyping. sgRNAs and HDR templates are listed in **Table S1**.

Murine R1/E ES cells were grown on a confluent feeder layer of murine embryonic fibroblasts (MEFs) treated for 2 h with 10 µg/mL of mitomycin C (MMC; Sigma-Aldrich, M4287) and washed 3 times with DPBS (Life Technologies, 14190169). Approx. 30,000 R1/E ES cells per cm^2 were seeded on feeder cells in ESC medium (500 mL DMEM (Gibco, 41966-129), 90 mL FBS (PAN Biotech, Cat: P30-3302), 1.2 mL 50 mM β-Mercaptoethanol, 6 mL NEAA (Gibco, 11140-035), 6 mL Pen/Strep (Gibco, 15140-122), 90 µL LIF/ESGRO (Merck Millipore, ESG1107). Medium was changed daily, and every second day cells were split after detachment using 0.05% Trypsin-EDTA (Gibco, 25300-096). For transfection, 200,000 R1/E cells were seeded on MMC-treated feeder cells in a 6-well plate. On the next day, cells were transfected using Lipofectamine 3000 (Invitrogen, L3000001) and 0.75 µg pX458-TBM1 guide, 0.75 µg pX458-TBM2 guide, 0.75 µg TBM1 HDR template and 0.75 µg TBM2 HDR template according to the manufactures procedures. The day after transfection, EGFP-positive R1/E cells were sorted using a MoFlo cell sorter (Cytomation, Beckman Coulter) and EGFP-positive R1/E cells were enriched up to >90%. ~2000 EGFP-positive R1/E cells each were seeded on MEF feeder layer in 10 cm dishes and ES cell colonies were picked after 6-7 days. Single cell clones were split, with one part transferred to 96-well plates and the other used for preparation of genomic DNA for PCR genotyping to identify mutant alleles using WT- and mutation-specific PCR primers (see **Table S2** and real-time PCR (Light-Cycler, Roche Life Science). In the selected ES cell clones, genomic modifications were confirmed by sequencing.

ES cell clone 3-3/E10 containing correct homozygous alterations in both T6BMs was injected into 8-cell C57Bl6/Ncrl wildtype embryos by utilizing laser-assisted injection technology (*56*). Donor embryos were generated by natural mating. Two to three hours after ES-cell injection, 10-12 embryos were transferred into the oviduct of a pseudogravide Crl:CD1(IDR) female, and chimeric males were born with brown fur (>90% chimerism). After crossing to C57BL/6 animals, germline transmission and brown F1 generation yielded heterozygous *Malt1*$^{TBM/+}$ and homozygous *Malt1*$^{TBM/TBM}$ mice upon crossing. Genotypes were identified by differential PCR and mutations were verified by genomic sequencing (**Fig. 1B; Fig. 1D; Table S2**). The complete *Malt1* CDS was sequenced to verify that no additional mutations changing the coding sequence were found. sgRNAs and HDR templates are listed in **Table S1**.

Generation of *Malt1*$^{TBMPM/TBMPM}$ mice

Sperm from *Malt1*$^{TBM/+}$ mice was used for in vitro fertilization in C57BL/6N females (obtained from Charles River, Sulzbach, Germany) superovulated with 5 units PMSG (Pregnant Mare`s Serum Gonadotropin) and 5 units HCG (Human Chorionic Gonadotropin). Fertilized one cell embryos were edited by electroporation using a specific in vitro transcribed (EnGen® sgRNA Synthesis Kit, NEB, E3322, USA) single gRNA. Prior to electroporation, the sgRNA (200 ng/µl) and single strand oligonucleotide HDR template (ssODN, 300 ng/µl) were diluted in Opti-MEM buffer (Thermo Fisher Scientific, Germany) together with recombinant Cas9 protein (200 ng/µl, IDT, Coralville, USA) and incubated for 10 min at room temperature and 10 minutes at 37°C to form the active ribonucleoprotein (RNP) complex. Electroporation was performed using the NEPA21 electroporator and a CUY501P1-1.5 electrode (Nepa Gene Co., Ltd., Japan). Zygotes were transferred into pseudopregnant CD1 female mice to obtain live pups. Modification of the paracaspase site in offspring was detected via cleavage with BssHII (NEB, R0199S) and verified by sequencing (**Fig. S8B**). The silent single nucleotide polymorphism (SNP) c.1323A/c.1323G in exon 11, stemming from the ES cells used for TBM mouse generation, served as a marker for expression of C472A on the same allele as the TBM mutations. Crossing to C57BL6 yielded heterozygous Malt1$^{TBMPM/+}$ mice which were used for backcrossing and generation of homozygous Malt1$^{TBMPM/TBMPM}$ mice. sgRNAs and HDR templates are listed in **Table S1**.

Generation of *Malt1* floxed strain

Malt1 floxed (fl) mice were derived from the EUCOMM ES cell clone *Malt1*$^{tm1a(EUCOMM)Hmgu}$ (HEPD0618_3_D10), which was injected into blastocysts and transferred into foster mothers and the IRES-lacZ/Neo cassette was deleted by crossing to ROSA26-FLPe deleter mice (Tg(ACTFLPe)9205Dym) (*53*).

Mating and pairings

For conditional expression of the *Malt1* TBM allele in T cells, *Malt1*$^{TBM/+}$ were crossed to CD4-Cre (CD4-Cre (Tg(CD4-cre)1Cwi) (*47*) to yield *Malt1*$^{TBM/+}$;CD4-Cre, which were paired to *Malt1*$^{fl/fl}$ mice to yield *Malt1*$^{TBM/fl}$;CD4-Cre. For conditional expression of the *Malt1* TBM allele in Treg cells, *Malt1*$^{TBM/+}$ mice were crossed to *FoxP3-Cre* transgenic mice (Tg(Foxp3-EGFP/icre) (*48*) to yield

Malt1$^{TBM/+}$*;FoxP3-Cre*, which were paired to *Malt1*$^{fl/fl}$, yielding *Malt1*$^{TBM/fl}$;FoxP3-Cre (*Malt1* TBM-Treg). For Traf6$^{fl/fl}$;CD4-Cre (*Traf6*-ΔT) mice, frozen embryos of *Traf6*$^{tm2a(EUCOMM)Wtsi}$ (EMMA ID EM:08446; Infrafrontiers Biocenter Oulu) were transferred into foster mothers and the IRES-lacZ/Neo cassette was deleted by crossing to ROSA26-FLPe-deleter mice. *Traf6*$^{fl/fl}$ mice were crossed to CD4-Cre transgenic mice for T cell specific deletion of exons 4 and 5 of the *Traf6* locus. Genotyping primers are listed in **Table S2**. *Malt1*$^{-/-}$ mice were generated by crossing *Malt1* floxed mice to ROSA26-Cre deleter mice (*54*) for deletion of exon 3 resulting in a downstream frame shift.

MALT1 inhibitor treatment of *Traf6*-ΔT mice

MLT-985 stock solution was prepared at 40 mg/mL in DMSO and vortexed to solubilize. For injection, stock was diluted 1:20 in DPBS, yielding a crystalline suspension. 8 week old Traf6-ΔT mice were injected i.p. BID at 16 mg/kg in a volume of 200 µL per 25 g body weight over a 10 day period. Suspension was kept at 37°C prior to each injection. On day 11, lymphocyte populations were analyzed via flow cytometry and Western blot. See supplemental methods for Western blot methods.

Immune cell phenotyping by flow cytometry

Lymphocyte populations were analyzed from single-cell suspensions prepared from murine tissues (spleen, lymph nodes, thymus, or bone marrow). Tissue was collected from mice and meshed, treated with red blood cell lysis buffer (Miltenyi, 130-094-183), and 1 million cells were plated per staining. Cells were washed twice with PBS (350 x g, 5 min, 4°C) and dead cells were stained using eFluor780 dye (eBioscience, 65-0865-18, 1:1000 in PBS, 30 min, 4°C). Cells were washed with FCM buffer (3% FCS in PBS) and treated with anti-CD16/CD32 (Fc-block, eBioscience, 14-0161-85, 1:200 in FCM buffer, 20 min, RT, RRID: AB_467132). Supernatant was discarded and cells were stained with fluorescent antibodies for 20 min at RT. More detailed methodology and antibodies can be found in the Supplementary Materials.

Cell culture and stimulation

Jurkat T cells (RPMI 1640 Medium) and HEK293T cells (DMEM) supplemented 10% fetal calf serum, 100 U/ml penicillin and 100 µg/ml streptomycin were grown in humidified atmosphere (37°C, 5%

CO_2). Primary murine CD4 T cells were isolated from spleen using the CD4 T cell isolation kit II (Miltenyi) by negative magnetic-activated cell sorting (MACS) as described (*49*). More detailed methodology, stimulation and treatment of cells can be found in the Supplementary Materials.

***In vitro* MALT1 activity assay**

Full length MALT1B WT and E795A were cloned into the pGEX-6P-1 vector (Addgene) and recombinant protein was expressed in BL21 (DE3) competent E. coli cells (NEB) and ÄKTA purified via the N-terminal GST tag using a 1 mL GSTrap column (GE Healthcare). MALT1 kinetics were measured as described previously (*58*). Briefly, 200 ng of protein were diluted in cleavage buffer (MES (50 mM), NaCl (150 mM), Saccharose (10% w/v), CHAPS (0.1%), Tri-Na-Citrate (1 M), DTT (1 mM, added fresh), pH 7.0) and mixed with increasing concentrations of the fluorescent substrate AC-LRSR-AMC (Peptides International Inc.) in a 384-well microplate. Fluorescence was measured on a Synergy 2 Microplate Reader (Biotek) and reaction velocities were compared within the linear range.

Generation of knockout Jurkat T cells

Generation of MALT1-, BCL10- and CARD11-deficient Jurkat T cells has been described earlier (*3, 32, 50*). For generation of TRAF6 KO Jurkat T cells, sequences coding for sgRNAs targeting in Exon 1 and Exon 2 were cloned into vector px458, and transfected by electroporation in parental, BCL10 KO or CARD11 KO Jurkat T cells using 220 V and 1,000 µF utilizing a Gene Pulser X (BioRad), and sorted for GFP-expressing cells after 2 days using a MoFlow sorting system. After serial dilution and expansion of single clones, KO cell lines were confirmed by protein expression on WB. For generation of TRAF6/TCRα dKO Jurkat T cells, a guide targeting the TCRα constant region (TRAC) exon 1 was cloned into vector pX458 and transfected into TRAF6 KO Jurkat T cells as described above. KO cells were confirmed by anti-TCRα/β (1:200, #306722, BioLegend, RRID: AB_2562805) and anti-CD3ε (1:200, #300452, BioLegend, RRID: AB_2564148) staining by FACS. sgRNAs are listed in **Table S1**.

Lentiviral transduction of Jurkat T cells

For stable reconstitution of TRAF6- and MALT1-deficient Jurkat T cells, TRAF6 and MALT1 constructs were linked to hΔCD2 by a co-translational processing site T2A (*51*) and introduced into a

pHAGE transfer vector. Lentiviral NF-κB-EGFP reporter has been described (*49*). Lentiviral constructs for AP-1-mCherry (Addgene #118095) and NF-AT-EGFP (Addgene #118031) reporter constructs were cloned by transferring previously described retroviral reporters into pHAGE backbone (*52*). $2x10^6$ HEK293T cells were seeded in 10 cm² dishes and transfected with 1.5 µg psPAX2 (Addgene #12260), 1 µg pMD2.G (Addgene #12259) and 2 µg transfer vector using X-tremeGENE HP DNA Transfection Reagent (Roche). For transduction, virus-containing supernatant was applied to $5x10^5$ Jurkat T cells, mixed with Polybrene (8 µg/ml) and incubated for 24 hours. After transduction, cells were washed with PBS, resuspended in RPMI, cultured for ten days and expression of hΔCD2 determined by flow cytometry. Protein expression was confirmed by WB. For transient transfection, 8×10^6 Jurkat T cells were electroporated with 5 µg pCAGGS-E-tag hCYLD WT or R324A expression plasmid as described above. After cultivation for 48 hours cells were lysed in CoIP buffer and analyzed by WB. For generation of stable reporter cell line, Jurkat T cells were lentivirally transduced with the NF-κB-EGFP, AP1-mCherry or NF-AT-EGFP pHAGE reporter constructs as described above. Stimulation of reporter cells was performed in 500 µl medium in 24-well plates at 37°C, and EGFP or mCherry expression assessed and quantified by flow cytometry.

Analyses of cytokines and autoantibodies

Cytokines in sera of mice were measured according to manufacturer protocol via flow cytometry using a cytometric bead array kit (BD, 562246) and specific beads for the cytokines IL-4 (562272), IL-6 (562236), IL-10 (562263), IL-17 (562261), INFγ (562233), and TNFα (562336). Autoantibodies in serum of mice were measured according to manufacturer protocol via ELISA (Alpha Diagnostic International, 5110).

Statistical Analysis

For sample size determination of mouse experiments, we used Power analyses (t-tests) using G*Power Software and Binomial Distributions using R, type I error was set 0.05, type 2 error was set 0.10, Power was set 0.90, Cohen's effect size was approximated 1.66. All experiments in Jurkat T cells contained at least three biological replicates and values represent the mean ± standard error of the mean (SEM).

Experiments were analyzed by using unpaired Student's t-test with Welch's correction (Fig. 1-4 and 6; Fig. S2-S4 and S8) when only two groups were compared. One-way ANOVA combined with Tukey's Fig. 5A, Fig. 7, Fig. S7 C, D) or Dunnett's (Fig. 5E, G) multiple comparisons tests or two-way ANOVA combined with Sidak's multiple comparison test (Fig. 2O, P, Fig. S3K, L, Fig. S4G) were used when more than two groups were compared. Statistical significance is indicated by p-values. For quantification of active MALT1 upon biotin-MALT1 ABP pulldown, Fiji/ImageJ was used to calculate band intensity, and values from active MALT1 in the pull-down divided by total MALT1 in the lysate.

List of Supplementary Material

- Supplementary Materials and Methods
- Fig. S1: Generation and verification of MALT1 TBM mutant embryonic stem (ES) cells and mice.
- Fig. S2: Analysis of T cell numbers in *Malt1* TBM mice.
- Fig. S3: Staining of lymphocyte activation and Treg cell markers in *Malt1* TBM mice.
- Fig. S4: Phenotypic analysis of *Malt1* TBM-T, *Traf6*-ΔT and *Malt1* TBM-Treg mice.
- Fig. S5: Defective NF-κB and chronic MALT1 protease activation in *Malt1* TBM-T and *Traf6*-ΔT mice.
- Fig. S6: NF-κB activation and MALT1 protease activity upon loss of TRAF6-MALT1 interaction in Jurkat T cells.
- Fig. S7: NF-κB activation and MALT1 protease activity upon ablation of TRAF6 in Jurkat T cells.
- Fig. S8: Generation and analyses of *Malt1* TBMPM mice.
- Table S1: CRISPR guides and homology templates.
- Table S2: Genotyping primers.
- Table S3: Raw data file

References and Notes

1. M. Juilland, M. Thome, Holding All the CARDs: How MALT1 Controls CARMA/CARD-Dependent Signaling. *Frontiers in immunology* **9**, 1927 (2018).
2. J. Ruland, L. Hartjes, CARD-BCL-10-MALT1 signalling in protective and pathological immunity. *Nature reviews. Immunology* **19**, 118-134 (2019).
3. I. Meininger, R. A. Griesbach, D. Hu, T. Gehring, T. Seeholzer, A. Bertossi, J. Kranich, A. Oeckinghaus, A. C. Eitelhuber, U. Greczmiel, A. Gewies, M. Schmidt-Supprian, J. Ruland, T. Brocker, V. Heissmeyer, F. Heyd, D. Krappmann, Alternative splicing of MALT1 controls signalling and activation of CD4(+) T cells. *Nature communications* **7**, 11292 (2016).
4. A. Oeckinghaus, E. Wegener, V. Welteke, U. Ferch, S. C. Arslan, J. Ruland, C. Scheidereit, D. Krappmann, Malt1 ubiquitination triggers NF-kappaB signaling upon T-cell activation. *The EMBO journal* **26**, 4634-4645 (2007).

5. L. Sun, L. Deng, C. K. Ea, Z. P. Xia, Z. J. Chen, The TRAF6 ubiquitin ligase and TAK1 kinase mediate IKK activation by BCL10 and MALT1 in T lymphocytes. *Molecular cell* **14**, 289-301 (2004).
6. T. Klein, S. Y. Fung, F. Renner, M. A. Blank, A. Dufour, S. Kang, M. Bolger-Munro, J. M. Scurll, J. J. Priatel, P. Schweigler, S. Melkko, M. R. Gold, R. I. Viner, C. H. Regnier, S. E. Turvey, C. M. Overall, The paracaspase MALT1 cleaves HOIL1 reducing linear ubiquitination by LUBAC to dampen lymphocyte NF-kappaB signalling. *Nature communications* **6**, 8777 (2015).
7. J. Staal, Y. Driege, T. Bekaert, A. Demeyer, D. Muyllaert, P. Van Damme, K. Gevaert, R. Beyaert, T-cell receptor-induced JNK activation requires proteolytic inactivation of CYLD by MALT1. *The EMBO journal* **30**, 1742-1752 (2011).
8. F. Rebeaud, S. Hailfinger, A. Posevitz-Fejfar, M. Tapernoux, R. Moser, D. Rueda, O. Gaide, M. Guzzardi, E. M. Iancu, N. Rufer, N. Fasel, M. Thome, The proteolytic activity of the paracaspase MALT1 is key in T cell activation. *Nature immunology* **9**, 272-281 (2008).
9. B. Coornaert, M. Baens, K. Heyninck, T. Bekaert, M. Haegman, J. Staal, L. Sun, Z. J. Chen, P. Marynen, R. Beyaert, T cell antigen receptor stimulation induces MALT1 paracaspase-mediated cleavage of the NF-kappaB inhibitor A20. *Nature immunology* **9**, 263-271 (2008).
10. S. Hailfinger, H. Nogai, C. Pelzer, M. Jaworski, K. Cabalzar, J. E. Charton, M. Guzzardi, C. Decaillet, M. Grau, B. Dorken, P. Lenz, G. Lenz, M. Thome, Malt1-dependent RelB cleavage promotes canonical NF-kappaB activation in lymphocytes and lymphoma cell lines. *Proceedings of the National Academy of Sciences of the United States of America* **108**, 14596-14601 (2011).
11. K. M. Jeltsch, D. Hu, S. Brenner, J. Zoller, G. A. Heinz, D. Nagel, K. U. Vogel, N. Rehage, S. C. Warth, S. L. Edelmann, R. Gloury, N. Martin, C. Lohs, M. Lech, J. E. Stehklein, A. Geerlof, E. Kremmer, A. Weber, H. J. Anders, I. Schmitz, M. Schmidt-Supprian, M. Fu, H. Holtmann, D. Krappmann, J. Ruland, A. Kallies, M. Heikenwalder, V. Heissmeyer, Cleavage of roquin and regnase-1 by the paracaspase MALT1 releases their cooperatively repressed targets to promote T(H)17 differentiation. *Nature immunology* **15**, 1079-1089 (2014).
12. T. Uehata, H. Iwasaki, A. Vandenbon, K. Matsushita, E. Hernandez-Cuellar, K. Kuniyoshi, T. Satoh, T. Mino, Y. Suzuki, D. M. Standley, T. Tsujimura, H. Rakugi, Y. Isaka, O. Takeuchi, S. Akira, Malt1-induced cleavage of regnase-1 in CD4(+) helper T cells regulates immune activation. *Cell* **153**, 1036-1049 (2013).
13. D. Yamasoba, K. Sato, T. Ichinose, T. Imamura, L. Koepke, S. Joas, E. Reith, D. Hotter, N. Misawa, K. Akaki, T. Uehata, T. Mino, S. Miyamoto, T. Noda, A. Yamashita, D. M. Standley, F. Kirchhoff, D. Sauter, Y. Koyanagi, O. Takeuchi, N4BP1 restricts HIV-1 and its inactivation by MALT1 promotes viral reactivation. *Nature Microbiology* **4**, 1532-1544 (2019).
14. J. Ruland, G. S. Duncan, A. Wakeham, T. W. Mak, Differential requirement for Malt1 in T and B cell antigen receptor signaling. *Immunity* **19**, 749-758 (2003).
15. A. A. Ruefli-Brasse, D. M. French, V. M. Dixit, Regulation of NF-kappaB-dependent lymphocyte activation and development by paracaspase. *Science (New York, N.Y.)* **302**, 1581-1584 (2003).
16. F. Bornancin, F. Renner, R. Touil, H. Sic, Y. Kolb, I. Touil-Allaoui, J. S. Rush, P. A. Smith, M. Bigaud, U. Junker-Walker, C. Burkhart, J. Dawson, S. Niwa, A. Katopodis, B. Nuesslein-Hildesheim, G. Weckbecker, G. Zenke, B. Kinzel, E. Traggiai, D. Brenner, A. Brustle, M. St Paul, N. Zamurovic, K. D. McCoy, A. Rolink, C. H. Regnier, T. W. Mak, P. S. Ohashi, D. D. Patel, T. Calzascia, Deficiency of MALT1 paracaspase activity results in unbalanced regulatory and effector T and B cell responses leading to multiorgan inflammation. *Journal of immunology (Baltimore, Md. : 1950)* **194**, 3723-3734 (2015).
17. A. Demeyer, I. Skordos, Y. Driege, M. Kreike, T. Hochepied, M. Baens, J. Staal, R. Beyaert, MALT1 Proteolytic Activity Suppresses Autoimmunity in a T Cell Intrinsic Manner. *Frontiers in immunology* **10**, 1898 (2019).
18. A. Gewies, O. Gorka, H. Bergmann, K. Pechloff, F. Petermann, K. M. Jeltsch, M. Rudelius, M. Kriegsmann, W. Weichert, M. Horsch, J. Beckers, W. Wurst, M. Heikenwalder, T. Korn, V.

Heissmeyer, J. Ruland, Uncoupling Malt1 threshold function from paracaspase activity results in destructive autoimmune inflammation. *Cell reports* **9**, 1292-1305 (2014).
19. M. Jaworski, B. J. Marsland, J. Gehrig, W. Held, S. Favre, S. A. Luther, M. Perroud, D. Golshayan, O. Gaide, M. Thome, Malt1 protease inactivation efficiently dampens immune responses but causes spontaneous autoimmunity. *The EMBO journal* **33**, 2765-2781 (2014).
20. J. W. Yu, S. Hoffman, A. M. Beal, A. Dykon, M. A. Ringenberg, A. C. Hughes, L. Dare, A. D. Anderson, J. Finger, V. Kasparcova, D. Rickard, S. B. Berger, J. Ramanjulu, J. G. Emery, P. J. Gough, J. Bertin, K. P. Foley, MALT1 Protease Activity Is Required for Innate and Adaptive Immune Responses. *PloS one* **10**, e0127083 (2015).
21. M. Rosenbaum, A. Gewies, K. Pechloff, C. Heuser, T. Engleitner, T. Gehring, L. Hartjes, S. Krebs, D. Krappmann, M. Kriegsmann, W. Weichert, R. Rad, C. Kurts, J. Ruland, Bcl10-controlled Malt1 paracaspase activity is key for the immune suppressive function of regulatory T cells. *Nature communications* **10**, 2352 (2019).
22. M. C. Walsh, J. Lee, Y. Choi, Tumor necrosis factor receptor- associated factor 6 (TRAF6) regulation of development, function, and homeostasis of the immune system. *Immunol Rev* **266**, 72-92 (2015).
23. C. G. King, T. Kobayashi, P. J. Cejas, T. Kim, K. Yoon, G. K. Kim, E. Chiffoleau, S. P. Hickman, P. T. Walsh, L. A. Turka, Y. Choi, TRAF6 is a T cell-intrinsic negative regulator required for the maintenance of immune homeostasis. *Nat Med* **12**, 1088-1092 (2006).
24. H. Noels, G. van Loo, S. Hagens, V. Broeckx, R. Beyaert, P. Marynen, M. Baens, A Novel TRAF6 binding site in MALT1 defines distinct mechanisms of NF-kappaB activation by API2middle dotMALT1 fusions. *The Journal of biological chemistry* **282**, 10180-10189 (2007).
25. N. Kutukculer, T. Seeholzer, T. J. O'Neill, C. Grass, A. Aykut, N. E. Karaca, A. Durmaz, O. Cogulu, G. Aksu, T. Gehring, A. Gewies, D. Krappmann, Human immune disorder associated with homozygous hypomorphic mutation affecting MALT1B splice variant. *J Allergy Clin Immunol* **147**, 775-778 e778 (2021).
26. N. Rehage, E. Davydova, C. Conrad, G. Behrens, A. Maiser, J. E. Stehklein, S. Brenner, J. Klein, A. Jeridi, A. Hoffmann, E. Lee, U. Dianzani, R. Willemsen, R. Feederle, K. Reiche, J. Hackermüller, H. Leonhardt, S. Sharma, D. Niessing, V. Heissmeyer, Binding of NUFIP2 to Roquin promotes recognition and regulation of ICOS mRNA. *Nature communications* **9**, 299 (2018).
27. K. Essig, N. Kronbeck, J. C. Guimaraes, C. Lohs, A. Schlundt, A. Hoffmann, G. Behrens, S. Brenner, J. Kowalska, C. Lopez-Rodriguez, J. Jemielity, H. Holtmann, K. Reiche, J. Hackermüller, M. Sattler, M. Zavolan, V. Heissmeyer, Roquin targets mRNAs in a 3'-UTR-specific manner by different modes of regulation. *Nature communications* **9**, 3810 (2018).
28. K. Martin, U. Junker, E. Tritto, E. Sutter, T. Rubic-Schneider, H. Morgan, S. Niwa, J. Li, A. Schlapbach, D. Walker, M. Bigaud, C. Beerli, A. Littlewood-Evans, B. Rudolph, M. Laisney, D. Ledieu, K. Beltz, J. Quancard, F. Bornancin, N. Zamurovic Ribrioux, T. Calzascia, Pharmacological Inhibition of MALT1 Protease Leads to a Progressive IPEX-Like Pathology. *Frontiers in immunology* **11**, (2020).
29. M. Bardet, A. Unterreiner, C. Malinverni, F. Lafossas, C. Vedrine, D. Boesch, Y. Kolb, D. Kaiser, A. Gluck, M. A. Schneider, A. Katopodis, M. Renatus, O. Simic, A. Schlapbach, J. Quancard, C. H. Regnier, G. Bold, C. Pissot-Soldermann, J. M. Carballido, J. Kovarik, T. Calzascia, F. Bornancin, The T-cell fingerprint of MALT1 paracaspase revealed by selective inhibition. *Immunology and cell biology* **96**, 81-99 (2018).
30. A. C. Eitelhuber, O. Vosyka, D. Nagel, M. Bognar, D. Lenze, K. Lammens, F. Schlauderer, D. Hlahla, K. P. Hopfner, G. Lenz, M. Hummel, S. H. Verhelst, D. Krappmann, Activity-based probes for detection of active MALT1 paracaspase in immune cells and lymphomas. *Chemistry & biology* **22**, 129-138 (2015).

31. C. Pelzer, K. Cabalzar, A. Wolf, M. Gonzalez, G. Lenz, M. Thome, The protease activity of the paracaspase MALT1 is controlled by monoubiquitination. *Nature immunology* **14**, 337-345 (2013).
32. F. Schlauderer, T. Seeholzer, A. Desfosses, T. Gehring, M. Strauss, K. P. Hopfner, I. Gutsche, D. Krappmann, K. Lammens, Molecular architecture and regulation of BCL10-MALT1 filaments. *Nature communications* **9**, 4041 (2018).
33. J. W. Yu, P. D. Jeffrey, J. Y. Ha, X. Yang, Y. Shi, Crystal structure of the mucosa-associated lymphoid tissue lymphoma translocation 1 (MALT1) paracaspase region. *Proceedings of the National Academy of Sciences of the United States of America* **108**, 21004-21009 (2011).
34. K. Cabalzar, C. Pelzer, A. Wolf, G. Lenz, J. Iwaszkiewicz, V. Zoete, S. Hailfinger, M. Thome, Monoubiquitination and activity of the paracaspase MALT1 requires glutamate 549 in the dimerization interface. *PloS one* **8**, e72051 (2013).
35. Q. Yin, S. C. Lin, B. Lamothe, M. Lu, Y. C. Lo, G. Hura, L. Zheng, R. L. Rich, A. D. Campos, D. G. Myszka, M. J. Lenardo, B. G. Darnay, H. Wu, E2 interaction and dimerization in the crystal structure of TRAF6. *Nature structural & molecular biology* **16**, 658-666 (2009).
36. R. Galetto, C. Lebuhotel, L. Poirot, A. Gouble, M. L. Toribio, J. Smith, A. Scharenberg, Pre-TCRα supports CD3-dependent reactivation and expansion of TCRα-deficient primary human T-cells. *Molecular Therapy - Methods & Clinical Development* **1**, 14021 (2014).
37. J. Quancard, O. Simic, C. Pissot Soldermann, R. Aichholz, M. Blatter, M. Renatus, P. Erbel, S. Melkko, R. Endres, M. Sorge, L. Kieffer, T. Wagner, K. Beltz, P. McSheehy, M. Wartmann, C. H. Regnier, T. Calzascia, T. Radimerski, M. Bigaud, A. Weiss, F. Bornancin, A. Schlapbach, Optimization of the In Vivo Potency of Pyrazolopyrimidine MALT1 Protease Inhibitors by Reducing Metabolism and Increasing Potency in Whole Blood. *J Med Chem* **63**, 14594-14608 (2020).
38. C. Dumont, U. Sivars, T. Andreasson, L. Odqvist, J. Mattsson, A. DeMicco, K. Pardali, G. Johansson, L. Yrlid, R. J. Cox, F. Seeliger, M. Larsson, U. Gehrmann, A. M. Davis, O. Vaarala, A MALT1 inhibitor suppresses human myeloid DC, effector T-cell and B-cell responses and retains Th1/regulatory T-cell homeostasis. *PloS one* **15**, e0222548 (2020).
39. D. R. Myers, J. Zikherman, J. P. Roose, Tonic Signals: Why Do Lymphocytes Bother? *Trends in Immunology* **38**, 844-857 (2017).
40. K. Matsushita, O. Takeuchi, D. M. Standley, Y. Kumagai, T. Kawagoe, T. Miyake, T. Satoh, H. Kato, T. Tsujimura, H. Nakamura, S. Akira, Zc3h12a is an RNase essential for controlling immune responses by regulating mRNA decay. *Nature* **458**, 1185-1190 (2009).
41. C. G. Vinuesa, M. C. Cook, C. Angelucci, V. Athanasopoulos, L. Rui, K. M. Hill, D. Yu, H. Domaschenz, B. Whittle, T. Lambe, I. S. Roberts, R. R. Copley, J. I. Bell, R. J. Cornall, C. C. Goodnow, A RING-type ubiquitin ligase family member required to repress follicular helper T cells and autoimmunity. *Nature* **435**, 452-458 (2005).
42. K. U. Vogel, S. L. Edelmann, K. M. Jeltsch, A. Bertossi, K. Heger, G. A. Heinz, J. Zoller, S. C. Warth, K. P. Hoefig, C. Lohs, F. Neff, E. Kremmer, J. Schick, D. Repsilber, A. Geerlof, H. Blum, W. Wurst, M. Heikenwalder, M. Schmidt-Supprian, V. Heissmeyer, Roquin paralogs 1 and 2 redundantly repress the Icos and Ox40 costimulator mRNAs and control follicular helper T cell differentiation. *Immunity* **38**, 655-668 (2013).
43. T. Mino, Y. Murakawa, A. Fukao, A. Vandenbon, H.-H. Wessels, D. Ori, T. Uehata, S. Tartey, S. Akira, Y. Suzuki, Carola G. Vinuesa, U. Ohler, Daron M. Standley, M. Landthaler, T. Fujiwara, O. Takeuchi, Regnase-1 and Roquin Regulate a Common Element in Inflammatory mRNAs by Spatiotemporally Distinct Mechanisms. *Cell* **161**, 1058-1073 (2015).
44. M. Di Pilato, E. Y. Kim, B. L. Cadilha, J. N. Prussmann, M. N. Nasrallah, D. Seruggia, S. M. Usmani, S. Misale, V. Zappulli, E. Carrizosa, V. Mani, M. Ligorio, R. D. Warner, B. D. Medoff, F. Marangoni, A. C. Villani, T. R. Mempel, Targeting the CBM complex causes Treg cells to prime tumours for immune checkpoint therapy. *Nature* **570**, 112-116 (2019).

45. B. Namjou, C. B. Choi, I. T. Harley, M. E. Alarcon-Riquelme, J. A. Kelly, S. B. Glenn, J. O. Ojwang, A. Adler, K. Kim, C. J. Gallant, S. A. Boackle, L. A. Criswell, R. P. Kimberly, E. E. Brown, J. Edberg, G. S. Alarcon, A. M. Stevens, C. O. Jacob, G. S. Gilkeson, D. L. Kamen, B. P. Tsao, J. M. Anaya, E. M. Kim, S. Y. Park, Y. K. Sung, J. M. Guthridge, J. T. Merrill, M. Petri, R. Ramsey-Goldman, L. M. Vila, T. B. Niewold, J. Martin, B. A. Pons-Estel, T. J. Vyse, B. I. Freedman, K. L. Moser, P. M. Gaffney, A. H. Williams, M. E. Comeau, J. D. Reveille, C. Kang, J. A. James, R. H. Scofield, C. D. Langefeld, K. M. Kaufman, J. B. Harley, S. C. Bae, Evaluation of TRAF6 in a large multiancestral lupus cohort. *Arthritis and rheumatism* **64**, 1960-1969 (2012).

46. S. Raychaudhuri, B. P. Thomson, E. F. Remmers, S. Eyre, A. Hinks, C. Guiducci, J. J. Catanese, G. Xie, E. A. Stahl, R. Chen, L. Alfredsson, C. I. Amos, K. G. Ardlie, A. Barton, J. Bowes, N. P. Burtt, M. Chang, J. Coblyn, K. H. Costenbader, L. A. Criswell, J. B. Crusius, J. Cui, P. L. De Jager, B. Ding, P. Emery, E. Flynn, P. Harrison, L. J. Hocking, T. W. Huizinga, D. L. Kastner, X. Ke, F. A. Kurreeman, A. T. Lee, X. Liu, Y. Li, P. Martin, A. W. Morgan, L. Padyukov, D. M. Reid, M. Seielstad, M. F. Seldin, N. A. Shadick, S. Steer, P. P. Tak, W. Thomson, A. H. van der Helm-van Mil, I. E. van der Horst-Bruinsma, M. E. Weinblatt, A. G. Wilson, G. J. Wolbink, P. Wordsworth, D. Altshuler, E. W. Karlson, R. E. Toes, N. de Vries, A. B. Begovich, K. A. Siminovitch, J. Worthington, L. Klareskog, P. K. Gregersen, M. J. Daly, R. M. Plenge, Genetic variants at CD28, PRDM1 and CD2/CD58 are associated with rheumatoid arthritis risk. *Nature genetics* **41**, 1313-1318 (2009).

47. P. P. Lee, D. R. Fitzpatrick, C. Beard, H. K. Jessup, S. Lehar, K. W. Makar, M. Pérez-Melgosa, M. T. Sweetser, M. S. Schlissel, S. Nguyen, S. R. Cherry, J. H. Tsai, S. M. Tucker, W. M. Weaver, A. Kelso, R. Jaenisch, C. B. Wilson, A critical role for Dnmt1 and DNA methylation in T cell development, function, and survival. *Immunity* **15**, 763-774 (2001).

48. X. Zhou, L. T. Jeker, B. T. Fife, S. Zhu, M. S. Anderson, M. T. McManus, J. A. Bluestone, Selective miRNA disruption in T reg cells leads to uncontrolled autoimmunity. *J Exp Med* **205**, 1983-1991 (2008).

49. T. Gehring, T. Erdmann, M. Rahm, C. Graß, A. Flatley, T. J. O'Neill, S. Woods, I. Meininger, O. Karayel, K. Kutzner, M. Grau, H. Shinohara, K. Lammens, R. Feederle, S. M. Hauck, G. Lenz, D. Krappmann, MALT1 Phosphorylation Controls Activation of T Lymphocytes and Survival of ABC-DLBCL Tumor Cells. *Cell reports* **29**, 873-888.e810 (2019).

50. T. Seeholzer, S. Kurz, F. Schlauderer, S. Woods, T. Gehring, S. Widmann, K. Lammens, D. Krappmann, BCL10-CARD11 Fusion Mimics an Active CARD11 Seed That Triggers Constitutive BCL10 Oligomerization and Lymphocyte Activation. *Frontiers in immunology* **9**, 2695 (2018).

51. K. Hadian, R. A. Griesbach, S. Dornauer, T. M. Wanger, D. Nagel, M. Metlitzky, W. Beisker, M. Schmidt-Supprian, D. Krappmann, NF-kappaB essential modulator (NEMO) interaction with linear and lys-63 ubiquitin chains contributes to NF-kappaB activation. *The Journal of biological chemistry* **286**, 26107-26117 (2011).

52. S. Jutz, J. Leitner, K. Schmetterer, I. Doel-Perez, O. Majdic, K. Grabmeier-Pfistershammer, W. Paster, J. B. Huppa, P. Steinberger, Assessment of costimulation and coinhibition in a triple parameter T cell reporter line: Simultaneous measurement of NF-κB, NFAT and AP-1. *J Immunol Methods* **430**, 10-20 (2016).

53. C. I. Rodríguez, F. Buchholz, J. Galloway, R. Sequerra, J. Kasper, R. Ayala, A. F. Stewart, S. M. Dymecki, High-efficiency deleter mice show that FLPe is an alternative to Cre-loxP. *Nature genetics* **25**, 139-140 (2000).

54. P. Soriano, Generalized lacZ expression with the ROSA26 Cre reporter strain. *Nature genetics* **21**, 70-71 (1999).

55. J. G. Doench, N. Fusi, M. Sullender, M. Hegde, E. W. Vaimberg, K. F. Donovan, I. Smith, Z. Tothova, C. Wilen, R. Orchard, H. W. Virgin, J. Listgarten, D. E. Root, Optimized sgRNA design to maximize activity and minimize off-target effects of CRISPR-Cas9. *Nat Biotechnol* **34**, 184-191 (2016).

56. W. T. Poueymirou, W. Auerbach, D. Frendewey, J. F. Hickey, J. M. Escaravage, L. Esau, A. T. Doré, S. Stevens, N. C. Adams, M. G. Dominguez, N. W. Gale, G. D. Yancopoulos, T. M. DeChiara, D. M. Valenzuela, F0 generation mice fully derived from gene-targeted embryonic stem cells allowing immediate phenotypic analyses. *Nat Biotechnol* **25**, 91-99 (2007).
57. P. Bankhead, M. B. Loughrey, J. A. Fernández, Y. Dombrowski, D. G. McArt, P. D. Dunne, S. McQuaid, R. T. Gray, L. J. Murray, H. G. Coleman, J. A. James, M. Salto-Tellez, P. W. Hamilton, QuPath: Open source software for digital pathology image analysis. *Sci Rep* **7**, 16878 (2017).
58. D. Nagel, S. Spranger, M. Vincendeau, M. Grau, S. Raffegerst, B. Kloo, D. Hlahla, M. Neuenschwander, J. Peter von Kries, K. Hadian, B. Dorken, P. Lenz, G. Lenz, D. J. Schendel, D. Krappmann, Pharmacologic inhibition of MALT1 protease by phenothiazines as a therapeutic approach for the treatment of aggressive ABC-DLBCL. *Cancer cell* **22**, 825-837 (2012).

Acknowledgments: We thank Johanna Grosch and Christiane Zgorzelski for excellent technical assistance, the HMGU monoclonal antibody facility (Regina Feederle) for providing antibodies and Jens Staal for providing CYLD constructs. We thank Ludger Klein, Andrea Oeckinghaus and Marc Schmidt-Supprian for helpful discussions. We thank the Wellcome Trust Sanger Institute Mouse Genetics Project (Sanger MGP) and its funders for providing the mutant mouse line *Traf6*$^{tm2a(EUCOMM)Wtsi}$ (Infrafrontiers Biocenter Oulu).

Funding: The work was funded by Helmholtz Zentrum München - German Research Center for Environmental Health. Work of D.K. was supported by Deutsche Forschungsgemeinschaft (ID 210592381 – SFB 1054 A04, ID 360372040 – SFB 1335 P07) and Deutsche Krebshilfe (No 70112622). V.H. was supported by the Deutsche Forschungsgemeinschaft SPP-1935 and SFB-1054 (ID 210592381 A03) as well as grants from the Wilhelm Sander (No 2018.082.1) and Deutsche Krebshilfe (No 70113538) foundations. Work of J.R. was supported by the Deutsche Forschungsgemeinschaft (ID 210592381 – SFB 1054, ID 360372040 – SFB 1335, ID 395357507 – SFB 1371, ID 369799452 – TRR 237, ID 452881907 – TRR 338, RU 695/9-1), European Research Council (ERC) under the European Union's Horizon 2020 research and innovation program (No 834154). W.W. was supported by Deutsche Forschungsgemeinschaft SFB 870.

Author Contributions: T.J.O, T.S., A.G. and D.K. conceived the study and designed experiments. T.J.O and A.G. designed targeting strategy in murine ES cells and zygotes and performed most immune phenotyping analyses in mice. T.S. conducted most biochemical and mechanistic analyses in primary and Jurkat T cells. T.G. optimized and performed analyses of MALT1 targets and helped with

phenotypic analyses. F.G. and W.W. performed CRISPR/Cas9 editing in zygotes and helped to establish mutant transgenic lines. I.H. and O.P. synthesized and provided MALT1 inhibitors. C.G. and M.J.T. generated Jurkat KO T cell clones, helped with reporter assays and molecular analyses. H.S. and V.H. helped with analyses of MALT1 targets. K.K, T.P. and M.K. performed histological analyses. K.D. and M.G. helped with generation and analyses of transgenic mice. M.R., T.Sch. and J.R. helped with image stream analyses and performed Treg suppressor experiments. R.N. performed laser-assisted ES cell injection in murine 8-cell embryo stages. T.J.O, T.S., A.G. and D.K. wrote the manuscript. All authors discussed, read and acknowledged the manuscript.

Competing Interests: D.K. is a scientific advisor of Monopteros Therapeutics Inc, Boston. The authors declare no conflict of interest. D.K., T.J.O, T.S., A.G. and C.G. are inventors on patent application EP21172676.5 submitted by Helmholtz Zentrum München that covers a method for constitutive MALT1 protease activation.

Data and materials availability: All data needed to evaluate the conclusions in this paper are available in the main text or the supplementary materials. Transgenic mice (Malt1 TBM and Malt1 TBMPM) are available from corresponding author under a material agreement with Helmholtz Zentrum München.

FIGURE LEGENDS

Fig. 1: *Malt1* TBM mice develop an early onset and fatal inflammatory disease. (A) Scheme of Glu (E) to Ala (A) exchanges in the T6BMs of MALT1A and MALT1B in *Malt1* TBM mice. (B) Identification of *Malt1*$^{+/+}$, *Malt1*$^{TBM/+}$ and *Malt1*$^{TBM/TBM}$ mice by PCR genotyping. (C) MALT1 protein expression in CD4+ T cells of *Malt1*$^{+/+}$, *Malt1*$^{TBM/+}$ and *Malt1*$^{TBM/TBM}$ mice by WB. (D) Survival curves of *Malt1*$^{TBM/TBM}$ mice and *Malt1*$^{TBM/+}$ littermates (n=10). (E) Representative histological pictures of hematoxylin and eosin staining of organs from *Malt1*$^{TBM/+}$ and *Malt1*$^{TBM/TBM}$ mice (25 to 29 days old). Scale bars: 50 µm. (F) Mouse weights of *Malt1*$^{TBM/+}$ and *Malt1*$^{TBM/TBM}$ mice. (G) Representative picture of spleens and lymph nodes (scale bar 1 cm) and spleen weights from *Malt1*$^{TBM/+}$ and *Malt1*$^{TBM/TBM}$ mice. (H) Concentrations of indicated inflammatory cytokines in the sera of *Malt1*$^{TBM/+}$ and *Malt1*$^{TBM/TBM}$ mice. Analyses in (C and F to H) were performed with animals at day 18 after birth and heterozygous *Malt1*$^{TBM/+}$ littermates (black) were compared to *Malt1*$^{TBM/TBM}$ mice (green). Each dot represents one mouse (five to twelve mice per group). All bars show the mean ± SEM and p-values were calculated by unpaired t-test with Welch's correction. Statistics for survival were calculated using a log-rank test. DD: death domain, Ig: Immunoglobulin domain, T6BM: TRAF6 binding mutant.

Fig. 2: Immune phenotyping reveals aberrant immune homeostasis in *Malt1* TBM mice. (A to D) Flow cytometric analysis of CD3+ and B220+ lymphocytes (A) and quantifications showing total (B) or relative (C and D) numbers in spleen (SPL), lymph nodes (LN), thymus (THY) or bone marrow (BM) in *Malt1*$^{TBM/+}$ and *Malt1*$^{TBM/TBM}$ mice. (E to J) Flow cytometric analysis of CD44, CD62L on CD4+ (E) or CD8+ (H) T cells and relative numbers of CD44^{hi}CD62L^{lo} CD4+ (F) and CD8+ (I) T_{EM} cells and relative numbers of naïve ($T_{naïve}$: CD44^{lo}CD62L^{hi}), central memory (T_{CM}: CD44^{hi}CD62L^{hi}), and T_{EM} CD4+ (G) and CD8+ (J) T cells from SPL of *Malt*1$^{TBM/+}$ and *Malt1*$^{TBM/TBM}$ mice. (K to N) Flow cytometric analysis of FoxP3+CD4+ Treg cells (K) and relative numbers of Treg cells (L), effector (e)Treg cells (CD4+CD44^{hi}CD62L^{lo}) (M) and expression of CTLA-4 and OX40 on eTreg cells (MFI) in SPL of *Malt1*$^{TBM/+}$ and *Malt1*$^{TBM/TBM}$ mice. (O and P) Spleen weight (O) and relative numbers of CD4+ and CD8+ T_{EM} (CD44^{hi}CD62L^{lo}) cells in SPL (P) of *Malt1*$^{+/+}$ and *Malt1*$^{TBM/TBM}$ *littermates* at an age of 3, 6 or 12 month. Analyses in A to N were performed with animals at day 18 after birth and

heterozygous *Malt1*$^{TBM/+}$ littermates (black) were compared to *Malt1*$^{TBM/TBM}$ mice (green). Each dot represents one mouse (B-N: five to eleven mice per group, O, P: three to eleven mice per group). All bars show the mean ± SEM and p-values were calculated by unpaired t-test with Welch's correction (B, C, D, E, F, I, L, M and N) or two-way analysis of variance (ANOVA) combined with Sidak's multiple comparisons test (O and P).

Fig. 3: Activation of T cells in *Malt1* TBM-T and *Traf6*-ΔT but not *Malt1* TBM-Treg mice. (A and C) MALT1 (A) and TRAF6 (C) protein expression in CD4+ T cells of control and *Malt1* TBM-T or *Traf6*-ΔT mice by WB. (B) Representative histological picture of hematoxylin and eosin staining of tail from *Malt1*$^{+/+}$ and *Malt*1 TBM-T mouse showing epidermal inflammation in skin eczema at the tail. Scale bar 50 µm. (D to F) Spleen weight (D) and relative numbers of CD4+ (E) and CD8+ (F) T cells in control*, *Malt*1 TBM-T, *Traf6*-ΔT and *Malt1* TBM-Treg mice. (G to L) Flow cytometric analysis of CD44, CD62L on CD4+ (G) or CD8+ (J) T cells, relative numbers of CD44^{hi}CD62L^{lo} CD4+ (H) and CD8+ (K) T_{EM} cells and relative numbers of $T_{naïve}$ (CD44^{lo}CD62L^{hi}), T_{CM} (CD44^{hi}CD62L^{hi}) and T_{EM} CD4+ (I) and CD8+ (L) T cells from SPL of control, *Malt*1 TBM-T, *Traf6*-ΔT and *Malt1* TBM-Treg mice. (M to O) Relative numbers of CD4+FoxP3+ Treg cells (M), eTreg cells (N) and OX40 expression (MFI) on eTreg cells from SPL of control, *Malt*1 TBM-T, *Traf6*-ΔT and *Malt1* TBM-Treg mice. (P and Q) Relative numbers of CD69+B220+ B cells (P) and fold change of CD86 MFI on B220+ B cells (Q) from control, *Malt*1 TBM-T and *Traf6*-ΔT. (R) Concentrations of anti-dsDNA immunoglobulin in sera of control, *Malt1* TBM-T and *Traf6*-ΔT mice. All analyses were done with mice at 11 to 13 weeks of age. *Littermate control mice were *Malt1*$^{fl/+}$*;CD4-Cre-, Malt1*$^{fl/+}$;CD4-Cre+ and *Malt1*$^{TBM/fl}$*;CD4-Cre-* or *Traf6*$^{fl/+}$*;CD4-Cre+, Traf6*$^{fl/fl}$*;CD4-Cre-* and *Traf6*$^{fl/+}$*;CD4-Cre- or Malt1*$^{fl/+}$*;FoxP3-Cre-, Malt1*$^{fl/+}$;FoxP3-Cre+ and *Malt1*$^{TBM/fl}$*;FoxP3-Cre-* (black) for *Malt1* TBM-T (blue) or *Traf6*-ΔT (rose) or *Malt1* TBM-Treg (yellow), respectively. Each dot represents one mouse (D-Q: five to six mice per group, R: five to eleven mice per group). All bars show the mean ± SEM and p-values were calculated by unpaired t-test with Welch's correction.

Fig. 4: Defective NF-κB and chronic MALT1 protease activation in *Malt1* TBM-T and *Traf6*-ΔT mice. (A, B, G and H) Analyses of P/I-inducible NF-κB DNA binding (EMSA), canonical NF-κB

signaling and MALT1 substrate cleavage (WB) (A and B) and constitutive MALT1 substrate cleavage (WB) (G and H) in splenic CD4+ T cells from control, *Malt1* TBM-T (A and G) and *Traf6*-ΔT (B and H) mice. Asterisks indicate unspecific signals. (C to F) Image stream analyses showing representative pictures (BF: bright field; scale bars: 10 μm) (C), histograms showing similarity scores of p65 and DAPI stain (D and E) and quantification of p65 and DAPI similarity scores (F) in splenic CD4+ T cells of control, *Malt1* TBM-T and *Traf6*-ΔT mice after P/I stimulation (n=2, independent experiments). Non-stimulated (ns: grey) and P/I-stimulated (black) WT control CD4+ T cells are depicted (D-F). (I and J) Expression of IκBNS and ICOS in CD4+ (I) and CD8+ (J) T cells by flow cytometric analysis of spleen of control, *Malt1* TBM-T and *Traf6*-ΔT mice. All analyses were done with mice at 11 to 13 weeks of age. Littermate control mice were *Malt1*$^{fl/+}$*;CD4-Cre-, Malt1*$^{fl/+}$;CD4-Cre+ and *Malt1*$^{TBM/fl}$*;CD4-Cre-* or *Traf6*$^{fl/+}$*;CD4-Cre+, Traf6*$^{fl/fl}$*;CD4-Cre-* and *Traf6*$^{fl/+}$*;CD4-Cre-* for *Malt1* TBM-T or *Traf6*-ΔT, respectively. Each dot represents one mouse (I-J: six to twelve mice per group). All bars show the mean ± SEM and p-values were calculated by unpaired t-test with Welch's correction.

Fig. 5: TRAF6 counteracts cell autonomous constitutive MALT1 protease activation in T cells. (A and G) Detection of active MALT1 in reconstituted MALT1 KO (A) or TRAF6 KO (G) Jurkat T cells by labeling with biotin-MALT1 ABP and substrate cleavage in WB. For quantification, the ratio of active (pulldown) to total (lysate) MALT1 was determined (n=3, independent experiments). (B) MALT1 KO Jurkat cells reconstituted with MALT1B WT and respective mutants alone or in combination with the T6BM mutant (E795A) were untreated or P/I stimulated (60 min) and MALT1 activity was detected by biotin-MALT1-ABP assay and substrate cleavage in WB. (C) MALT1 KO Jurkat cells were reconstituted with MALT1B WT, E795A or E795D and analyzed for NF-κB signaling and MALT1 substrate cleavage in WB. (D) MALT1 KO Jurkat cells transduced with MALT1B E795D and increasing concentrations of MALT1A WT were analyzed for MALT1 substrate cleavage by WB. (E and F) Parental and TRAF6 KO Jurkat T cells were stimulated with P/I or αCD3/28 and NF-κB activation was determined by NF-κB-EGFP reporter assays (three to four replicates) (E) and MALT1 protease activity (F) by WB and MALT1-ABP PD. (G) MALT1 protease activity determined by MALT1-ABP PD in resting TRAF6 KO Jurkat T cells (three replicates). (H) TRAF6 KO Jurkat T cells

reconstituted with mock, TRAF6 WT or C70A were analyzed for NF-κB signaling and MALT1 substrate cleavage with and without P/I stimulation. Active MALT1 was detected by biotin-MALT1 ABP assay. (I) TRAF6 KO and TRAF6/BCL10 or TRAF6/CARD11 double KO (dKO) Jurkat T cells were analyzed for MALT1 substrate cleavage by WB. (J and K) Flow cytometric analysis showing loss of TCRα/β and CD3ε expression on TCRα/TRAF6 dKO Jurkat T cells (J) and analyses of MALT1 substrate cleavage in TCRα/TRAF6 dKO cells by WB (K). Bars show the mean ± SEM and p-values were calculated by ordinary one-way analysis of variance (ANOVA) combined with Tukey's (A) or Dunnett's (E, G) multiple comparisons test.

Fig. 6: Constitutive MALT1 protease activity drives lethal inflammation in *Malt1* TBM mice. (A and B) Identification of mutant alleles in mice by PCR genotyping (A) and MALT1 protein expression in splenocytes by WB (B). (C) Survival of *Malt1*$^{TBMPM/TBMPM}$ and*Malt1*$^{TBMPM/+}$ (13 mice per group) compared with *Malt1*$^{TBM/TBM}$ mice (as shown in Fig. 1D). (D) Mouse and spleen weights of *Malt1*$^{TBMPM/+}$ and *Malt1*$^{TBMPM/TBMPM}$ mice. (E) Analyses of NF-κB DNA binding (EMSA), NF-κB signaling and MALT1 substrate cleavage (WB) in isolated splenic CD4+ T cell (unstimulated and 30 min P/I stimulation) from *Malt1*$^{TBMPM/+}$ and *Malt1*$^{TBMPM/TBMPM}$ mice. Asterisk indicates unspecific signal. (F and G) Relative numbers of FoxP3+CD4+ Treg cells from SPL, LN and thymus (F) and B1 cells from peritoneal cavity (G) of *Malt1*$^{TBMPM/+}$ and *Malt1*$^{TBMPM/TBMPM}$ mice. (H) Relative numbers of CD44^{hi}CD62L^{lo} CD4+ and CD8+ T_{EM} cells in SPL and LN of *Malt1*$^{TBMPM/+}$ and *Malt1*$^{TBMPM/TBMPM}$ mice. (I) Concentration of IFNγ and TNFα in sera of *Malt1*$^{TBMPM/+}$ and *Malt1*$^{TBMPM/TBMPM}$ mice. All analyses were performed with animals at 8 weeks after birth. Each dot represents one mouse (five mice per group). All bars show the mean ± SEM and p-values were calculated by unpaired Student's *t*-test with Welch's correction. Statistics for survival were calculated using a log-rank test.

Fig. 7: MALT1 inhibitor treatment cures autoimmune phenotype of *Traf6*-ΔT mice. (A) TRAF6 KO Jurkat T cells were treated 24 h with indicated doses of MALT1 inhibitor MLT-943 or MLT-985 before analyses of MALT1 substrate cleavage by WB. (B) Schematic of MLT-985 treatment schedule of *Traf6*-ΔT mice starting 8 weeks after birth. (C) MALT1 substrate cleavage in isolated splenic CD4+ T cells from *Traf6*-ΔT mice treated with vehicle (n=3) or MLT-985 (n=4) analyzed by WB. Asterisk

indicates unspecific band. (D to H) Expression of IκBNS and ICOS in CD4+ (D), CD69 on CD3+ (E) and relative numbers of T_{EM} CD4+ and CD8+ T cells (F), CD4+Foxp3+ Treg cells (G) and MFI of OX40 expression on eTreg cells (H) from spleen of vehicle or MLT-985 treated *Traf6*-ΔT mice or WT mice (untreated). For vehicle (red) or MLT-985 (rose) *Traf6*$^{fl/fl}$*;CD4-Cre*+ (*Traf6*-ΔT) mice and WT mice each dot represents one mouse (three to four mice per group). All bars show the mean ± SEM and p-values were calculated by ordinary one-way analysis of variance (ANOVA) combined with Tukey's multiple comparisons test.

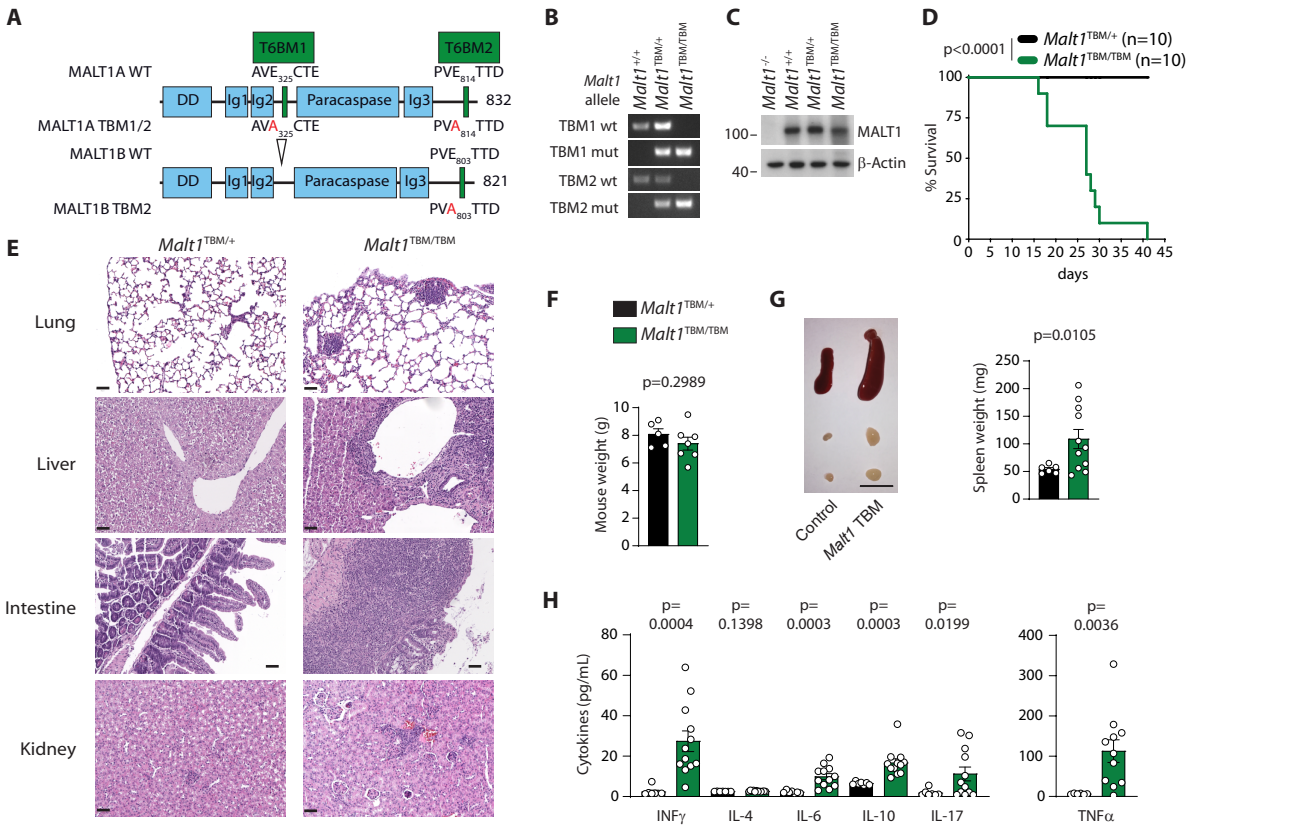
A
T6BM1
T6BM2
MALT1A WT
AVE325CTE
PVE814TTD
DD
Ig1
Ig2
Paracaspase
Ig3
832
MALT1A TBM1/2
AVA325CTE
PVA814TTD
MALT1B WT
PVE803TTD
821
MALT1B TBM2
PVA803TTD
B
Malt1 allele
Malt1+/+
Malt1TBM/+
Malt1TBM/TBM
TBM1 wt
TBM1 mut
TBM2 wt
TBM2 mut
C
Malt1-/-
Malt1+/+
Malt1TBM/+
Malt1TBM/TBM
100–
40–
MALT1
β-Actin
D
p<0.0001
Malt1TBM/+ (n=10)
Malt1TBM/TBM (n=10)
% Survival
days
E
Malt1TBM/+
Malt1TBM/TBM
Lung
Liver
Intestine
Kidney
F
Malt1TBM/+
Malt1TBM/TBM
p=0.2989
Mouse weight (g)
G
Control
Malt1 TBM
p=0.0105
Spleen weight (mg)
H
p= 0.0004
p= 0.1398
p= 0.0003
p= 0.0003
p= 0.0199
p= 0.0036
Cytokines (pg/mL)
INFγ
IL-4
IL-6
IL-10
IL-17
TNFα

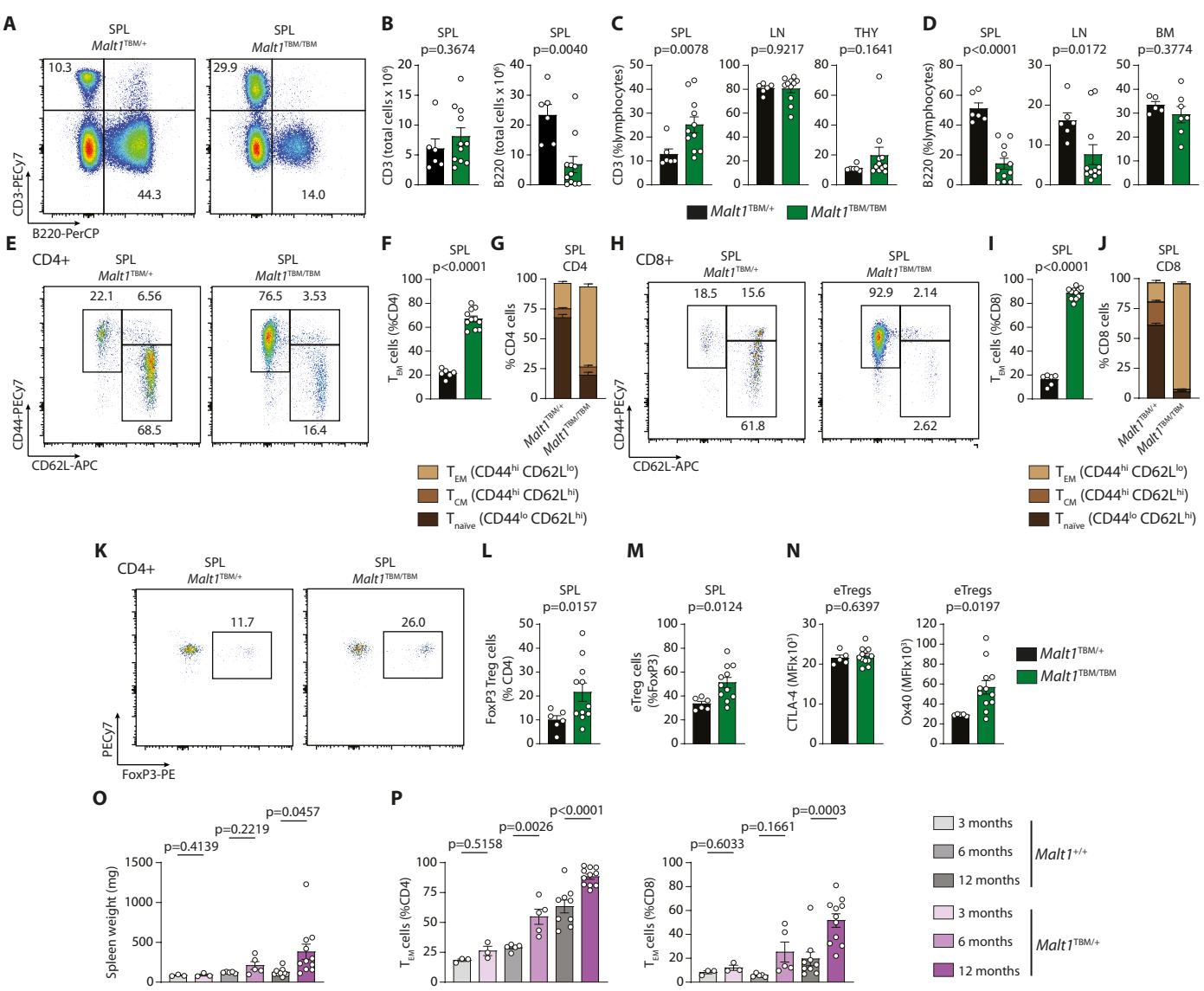
A
SPL
Malt1TBM/+
SPL
Malt1TBM/TBM
10.3
44.3
29.9
14.0
CD3-PECy7
B220-PerCP
B
SPL
p=0.3674
SPL
p=0.0040
CD3 (total cells x 10⁶)
B220 (total cells x 10⁶)
C
SPL
p=0.0078
LN
p=0.9217
THY
p=0.1641
CD3 (%lymphocytes)
D
SPL
p<0.0001
LN
p=0.0172
BM
p=0.3774
B220 (%lymphocytes)
Malt1TBM/+
Malt1TBM/TBM
E
CD4+
SPL
Malt1TBM/+
SPL
Malt1TBM/TBM
22.1
6.56
68.5
76.5
3.53
16.4
CD44-PECy7
CD62L-APC
F
SPL
p<0.0001
TEM cells (%CD4)
G
SPL
CD4
% CD4 cells
Malt1TBM/+
Malt1TBM/TBM
TEM (CD44hi CD62Llo)
TCM (CD44hi CD62Lhi)
Tnaïve (CD44lo CD62Lhi)
H
CD8+
SPL
Malt1TBM/+
SPL
Malt1TBM/TBM
18.5
15.6
61.8
92.9
2.14
2.62
CD44-PECy7
CD62L-APC
I
SPL
p<0.0001
TEM cells (%CD8)
J
SPL
CD8
% CD8 cells
Malt1TBM/+
Malt1TBM/TBM
TEM (CD44hi CD62Llo)
TCM (CD44hi CD62Lhi)
Tnaïve (CD44lo CD62Lhi)
K
CD4+
SPL
Malt1TBM/+
SPL
Malt1TBM/TBM
11.7
26.0
PECy7
FoxP3-PE
L
SPL
p=0.0157
FoxP3 Treg cells (% CD4)
M
SPL
p=0.0124
eTreg cells (%FoxP3)
N
eTregs
p=0.6397
eTregs
p=0.0197
CTLA-4 (MFIx10³)
Ox40 (MFIx10³)
Malt1TBM/+
Malt1TBM/TBM
O
p=0.4139
p=0.2219
p=0.0457
Spleen weight (mg)
P
p=0.5158
p=0.0026
p<0.0001
TEM cells (%CD4)
p=0.6033
p=0.1661
p=0.0003
TEM cells (%CD8)
3 months
6 months
12 months
Malt1+/+
3 months
6 months
12 months
Malt1TBM/+

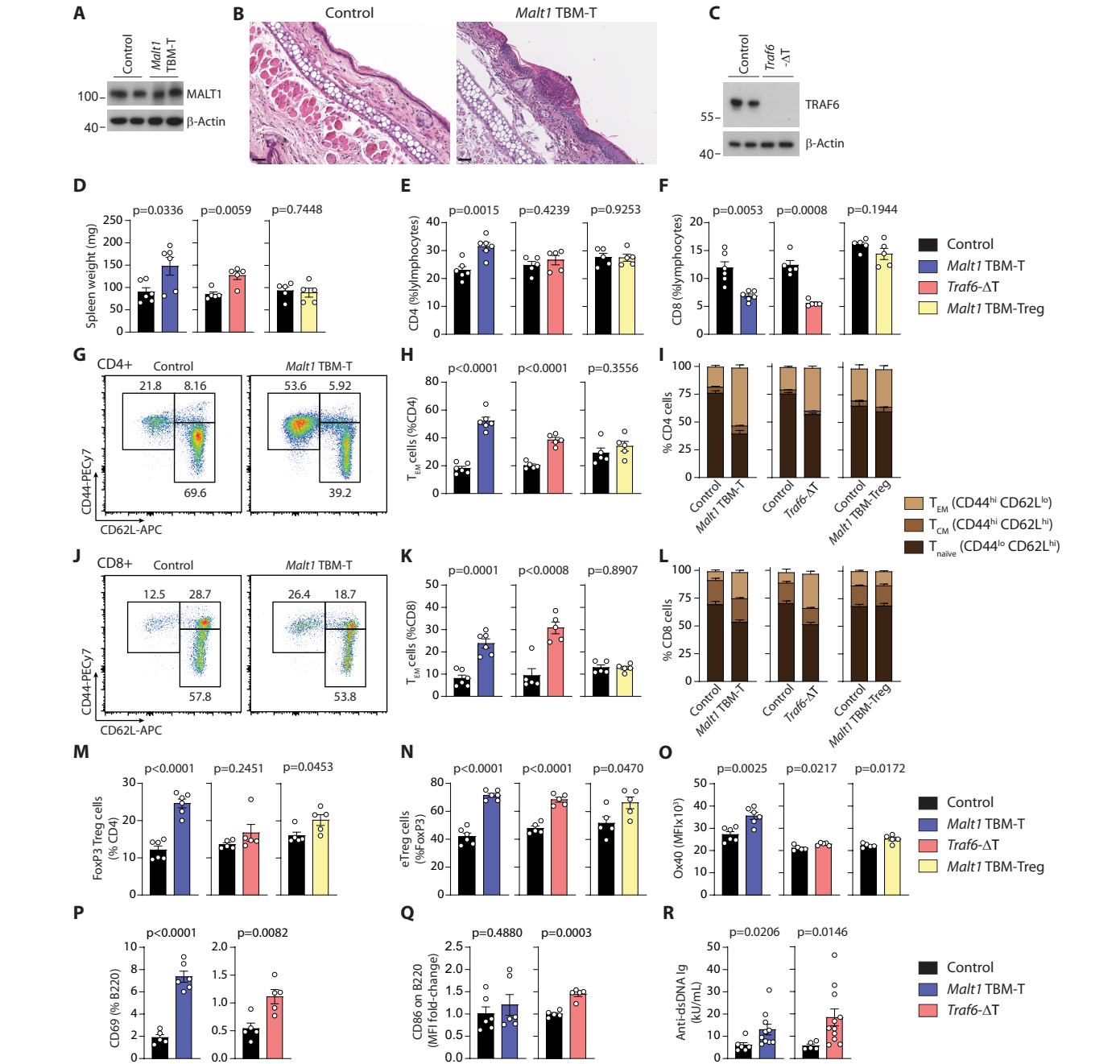
A
Control
Malt1 TBM-T
100–
40–
MALT1
β-Actin
B
Control
Malt1 TBM-T
C
Control
Traf6 -ΔT
55–
40–
TRAF6
β-Actin
D
Spleen weight (mg)
p=0.0336
p=0.0059
p=0.7448
E
CD4 (%lymphocytes)
p=0.0015
p=0.4239
p=0.9253
F
CD8 (%lymphocytes)
p=0.0053
p=0.0008
p=0.1944
Control
Malt1 TBM-T
Traf6-ΔT
Malt1 TBM-Treg
G
CD4+
Control
Malt1 TBM-T
21.8
8.16
69.6
53.6
5.92
39.2
CD44-PECy7
CD62L-APC
H
T_EM cells (%CD4)
p<0.0001
p<0.0001
p=0.3556
I
% CD4 cells
Control
Malt1 TBM-T
Control
Traf6-ΔT
Control
Malt1 TBM-Treg
T_EM (CD44^hi CD62L^lo)
T_CM (CD44^hi CD62L^hi)
T_naive (CD44^lo CD62L^hi)
J
CD8+
Control
Malt1 TBM-T
12.5
28.7
57.8
26.4
18.7
53.8
CD44-PECy7
CD62L-APC
K
T_EM cells (%CD8)
p=0.0001
p<0.0008
p=0.8907
L
% CD8 cells
Control
Malt1 TBM-T
Control
Traf6-ΔT
Control
Malt1 TBM-Treg
M
FoxP3 Treg cells (% CD4)
p<0.0001
p=0.2451
p=0.0453
N
eTreg cells (%FoxP3)
p<0.0001
p<0.0001
p=0.0470
O
Ox40 (MFIx10³)
p=0.0025
p=0.0217
p=0.0172
Control
Malt1 TBM-T
Traf6-ΔT
Malt1 TBM-Treg
P
CD69 (% B220)
p<0.0001
p=0.0082
Q
CD86 on B220 (MFI fold-change)
p=0.4880
p=0.0003
R
Anti-dsDNA Ig (kU/mL)
p=0.0206
p=0.0146
Control
Malt1 TBM-T
Traf6-ΔT

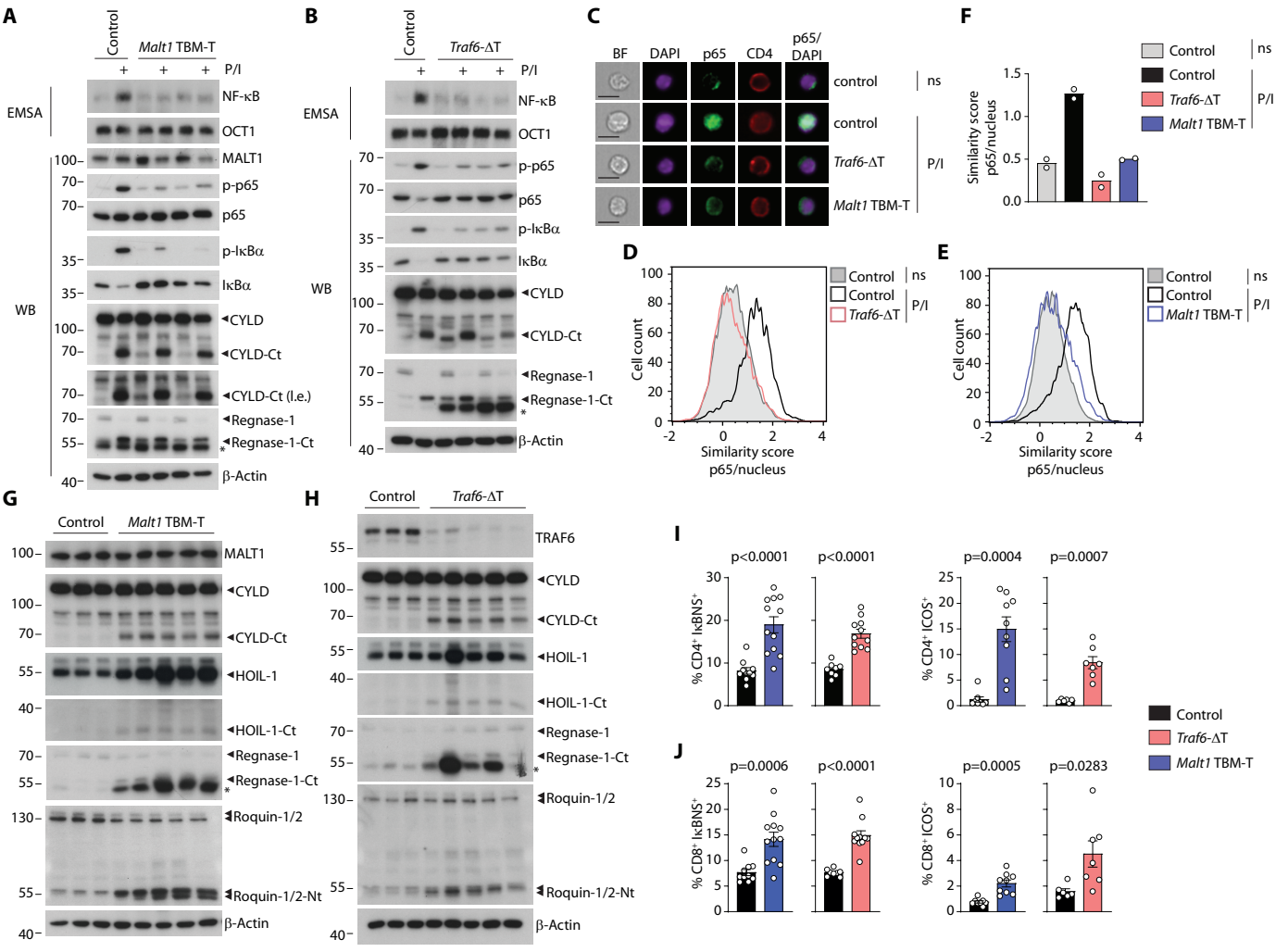
A
Control
Malt1 TBM-T
P/I
EMSA
NF-κB
OCT1
WB
MALT1
p-p65
p65
p-IκBα
IκBα
CYLD
CYLD-Ct
CYLD-Ct (l.e.)
Regnase-1
Regnase-1-Ct
β-Actin
B
Control
Traf6-ΔT
P/I
EMSA
NF-κB
OCT1
WB
p-p65
p65
p-IκBα
IκBα
CYLD
CYLD-Ct
Regnase-1
Regnase-1-Ct
β-Actin
C
BF
DAPI
p65
CD4
p65/ DAPI
control
control
Traf6-ΔT
Malt1 TBM-T
P/I
ns
D
Cell count
Similarity score p65/nucleus
Control
Control
Traf6-ΔT
ns
P/I
E
Cell count
Similarity score p65/nucleus
Control
Control
Malt1 TBM-T
ns
P/I
F
Similarity score p65/nucleus
Control
Control
Traf6-ΔT
Malt1 TBM-T
ns
P/I
G
Control
Malt1 TBM-T
MALT1
CYLD
CYLD-Ct
HOIL-1
HOIL-1-Ct
Regnase-1
Regnase-1-Ct
Roquin-1/2
Roquin-1/2-Nt
β-Actin
H
Control
Traf6-ΔT
TRAF6
CYLD
CYLD-Ct
HOIL-1
HOIL-1-Ct
Regnase-1
Regnase-1-Ct
Roquin-1/2
Roquin-1/2-Nt
β-Actin
I
p<0.0001
p<0.0001
p=0.0004
p=0.0007
% CD4+ IκBNS+
% CD4+ ICOS+
J
p=0.0006
p<0.0001
p=0.0005
p=0.0283
% CD8+ IκBNS+
% CD8+ ICOS+
Control
Traf6-ΔT
Malt1 TBM-T

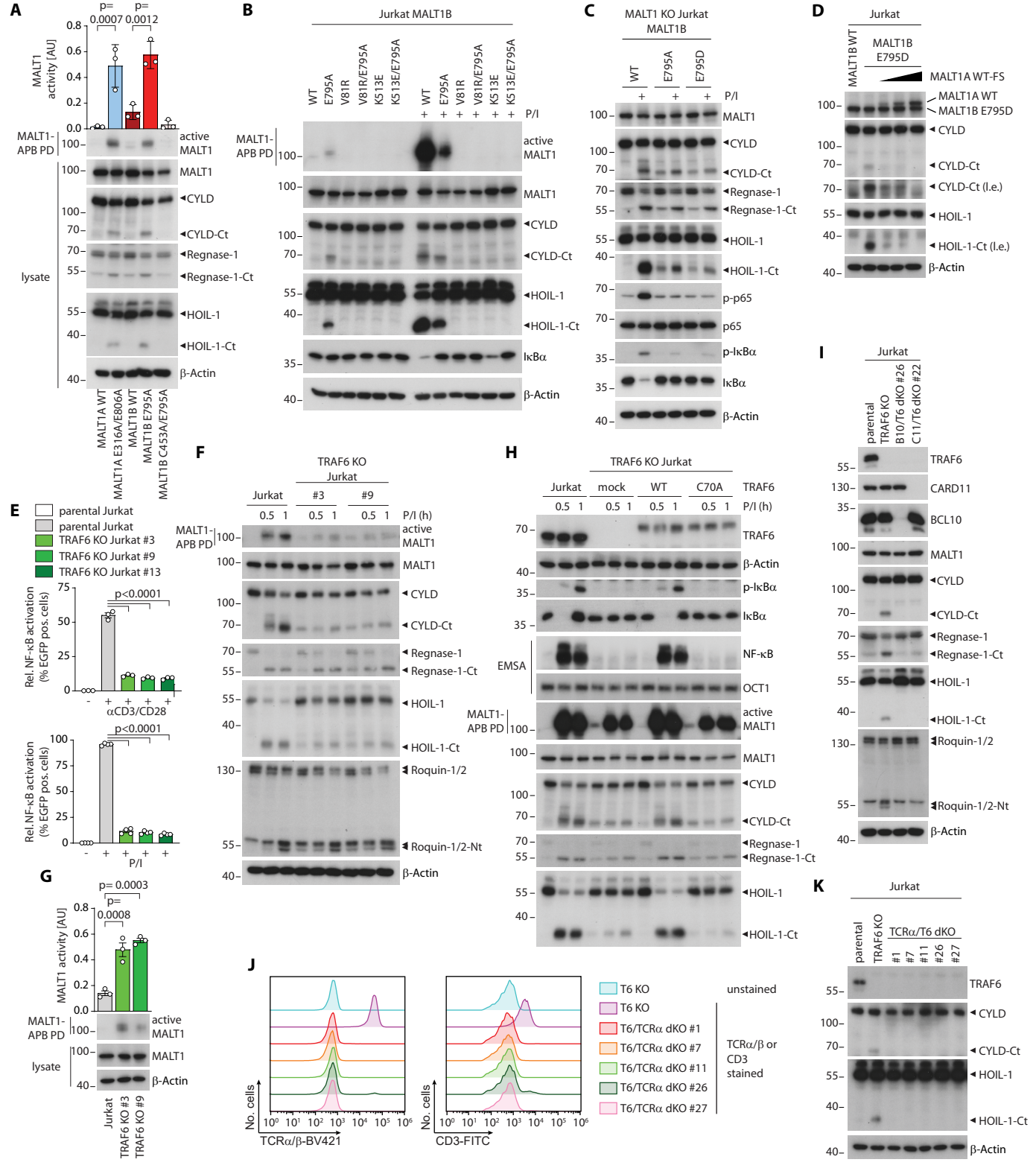
A
p= 0.0007
p= 0.0012
MALT1 activity [AU]
MALT1-APB PD
active MALT1
lysate
MALT1
CYLD
CYLD-Ct
Regnase-1
Regnase-1-Ct
HOIL-1
HOIL-1-Ct
β-Actin
MALT1A WT
MALT1A E316A/E806A
MALT1B WT
MALT1B E795A
MALT1B C453A/E795A
B
Jurkat MALT1B
WT
E795A
V81R
V81R/E795A
K513E
K513E/E795A
P/I
IκBα
C
MALT1 KO Jurkat MALT1B
p-p65
p65
p-IκBα
D
Jurkat
MALT1B WT
MALT1B E795D
MALT1A WT-FS
MALT1A WT
MALT1B E795D
HOIL-1-Ct (l.e.)
E
parental Jurkat
TRAF6 KO Jurkat #3
TRAF6 KO Jurkat #9
TRAF6 KO Jurkat #13
Rel.NF-κB activation (% EGFP pos. cells)
p<0.0001
αCD3/CD28
P/I
F
TRAF6 KO Jurkat
Jurkat
#3
#9
P/I (h)
Roquin-1/2
Roquin-1/2-Nt
G
p= 0.0003
p= 0.0008
Jurkat
TRAF6 KO #3
TRAF6 KO #9
H
TRAF6 KO Jurkat
mock
WT
C70A
TRAF6
EMSA
NF-κB
OCT1
I
parental
TRAF6 KO
B10/T6 dKO #26
C11/T6 dKO #22
BCL10
J
T6 KO
T6 KO
T6/TCRα dKO #1
T6/TCRα dKO #7
T6/TCRα dKO #11
T6/TCRα dKO #26
T6/TCRα dKO #27
unstained
TCRα/β or CD3 stained
No. cells
TCRα/β-BV421
CD3-FITC
K
TCRα/T6 dKO
#1
#7
#11
#26
#27

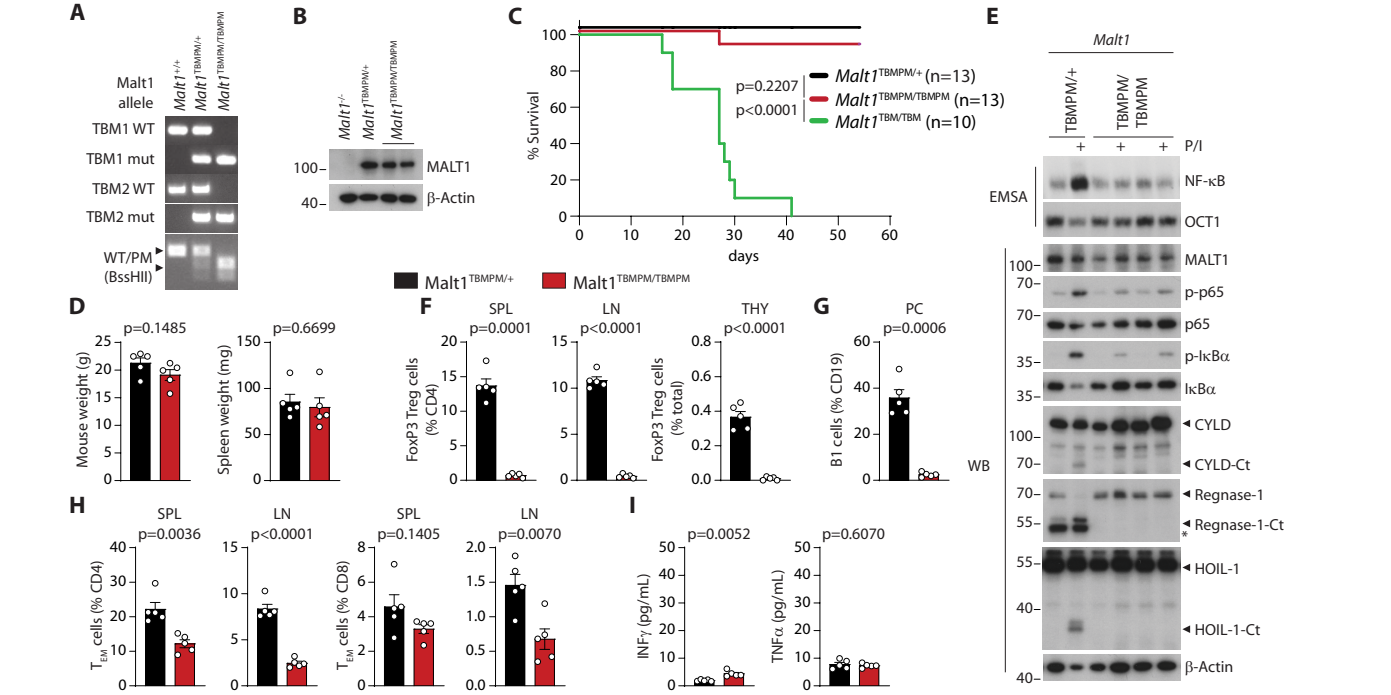
A
Malt1 allele
Malt1+/+
Malt1TBMPM/+
Malt1TBMPM/TBMPM
TBM1 WT
TBM1 mut
TBM2 WT
TBM2 mut
WT/PM
(BssHII)
B
Malt1-/-
Malt1TBMPM/+
Malt1TBMPM/TBMPM
100–
40–
MALT1
β-Actin
C
% Survival
days
p=0.2207
p<0.0001
Malt1TBMPM/+ (n=13)
Malt1TBMPM/TBMPM (n=13)
Malt1TBM/TBM (n=10)
Malt1TBMPM/+
Malt1TBMPM/TBMPM
D
p=0.1485
p=0.6699
Mouse weight (g)
Spleen weight (mg)
F
SPL
LN
THY
p=0.0001
p<0.0001
p<0.0001
FoxP3 Treg cells (% CD4)
FoxP3 Treg cells (% total)
G
PC
p=0.0006
B1 cells (% CD19)
H
SPL
LN
SPL
LN
p=0.0036
p<0.0001
p=0.1405
p=0.0070
TEM cells (% CD4)
TEM cells (% CD8)
I
p=0.0052
p=0.6070
IFNγ (pg/mL)
TNFα (pg/mL)
E
Malt1
TBMPM/+
TBMPM/TBMPM
P/I
EMSA
NF-κB
OCT1
WB
MALT1
p-p65
p65
p-IκBα
IκBα
CYLD
CYLD-Ct
Regnase-1
Regnase-1-Ct
HOIL-1
HOIL-1-Ct
β-Actin

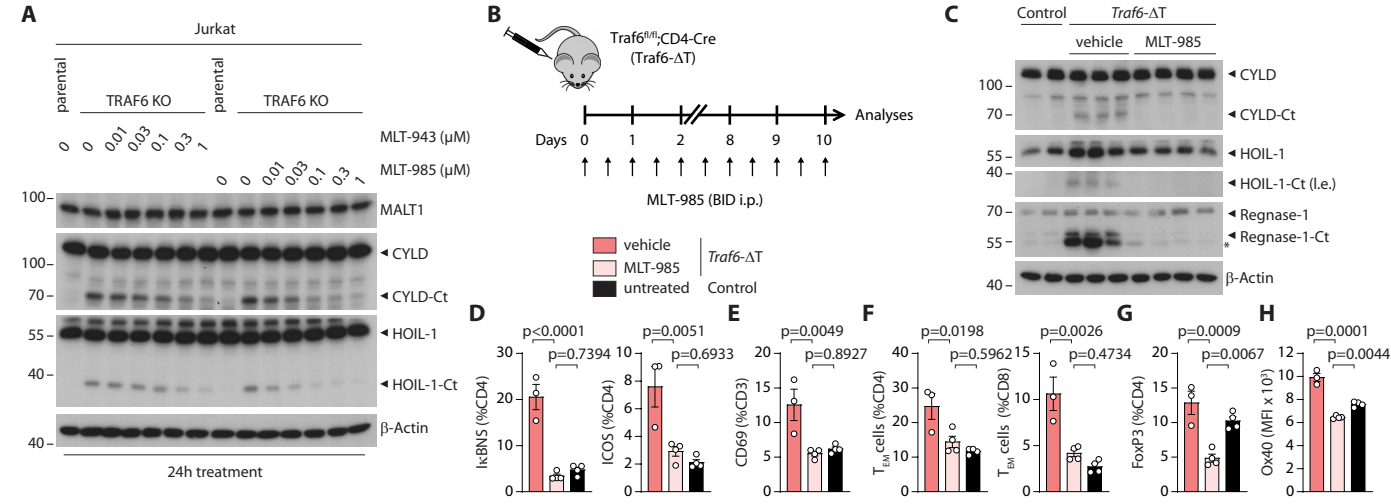
A
Jurkat
parental
TRAF6 KO
parental
TRAF6 KO
MLT-943 (μM)
MLT-985 (μM)
0 0 0.01 0.03 0.1 0.3 1
0 0 0.01 0.03 0.1 0.3 1
100
MALT1
100
70
CYLD
CYLD-Ct
55
40
HOIL-1
HOIL-1-Ct
40
β-Actin
24h treatment
B
Traf6fl/fl;CD4-Cre
(Traf6-ΔT)
Days 0 1 2 8 9 10
Analyses
MLT-985 (BID i.p.)
vehicle
MLT-985
untreated
Traf6-ΔT
Control
C
Control
Traf6-ΔT
vehicle
MLT-985
100
70
CYLD
CYLD-Ct
55
40
HOIL-1
HOIL-1-Ct (l.e.)
70
55
Regnase-1
Regnase-1-Ct
*
40
β-Actin
D
p<0.0001
p=0.7394
IκBNS (%CD4)
p=0.0051
p=0.6933
ICOS (%CD4)
E
p=0.0049
p=0.8927
CD69 (%CD3)
F
p=0.0198
p=0.5962
T EM cells (%CD4)
p=0.0026
p=0.4734
T EM cells (%CD8)
G
p=0.0009
p=0.0067
FoxP3 (%CD4)
H
p=0.0001
p=0.0044
Ox40 (MFI x 10³)

Supplementary Materials for

TRAF6 prevents fatal inflammation by homeostatic suppression of MALT1 protease

Thomas J. O'Neill et al.

Corresponding author: Daniel Krappmann, daniel.krappmann@helmholtz-muenchen.de

The PDF file includes:

Supplementary Materials and Methods
Figs. S1 to S8
Tables S1 and S2

Supplementary Materials and Methods

Antibodies for immune cell phenotyping

Staining was performed with anti-CD3-PECy7 (1:300, 25-0031-82, RRID: AB_469572), anti-CD45R-PerCP-Cy5.5 (1:200, Biolegend, 103234, AB_893353), anti-CD8a-FITC (1:100, 11-0081-85, RRID: AB_464916), anti-CD4-PE (1:300, 12-0042-85, RRID: AB_465512), anti-CD4-PerCP-Cy5.5 (1:300, 45-0042-82, RRID: AB_1107001), anti-CD44-PECy7 (1:400, 25-0441-82, RRID: AB_469623), anti-CD44-FITC (1:300, 11-0441-81, RRID: AB_465044), anti-CD62L-APC (1:300, BD Pharmingen, 553152, RRID: AB_398533), anti-CD86-FITC (1:100, 11-0862-82, RRID: AB_465148), anti-CD69-APC (1:200, 17-0691-82, RRID: AB_1210795), anti-Ox40-PECy7 (1:200, 25-1341-80, RRID: AB_2573395), anti-CTLA-4-PECy7 (1:200, Biolegend, 106313, RRID: AB_2564237), anti-CD19-APC (1:200, Elabscience, E-AB-F0986UE), anti-CD23-Biotin (1:300, 13-0232-81, RRID: AB_466392), anti-Strepdavadin-APC (1:100, 17-4317-82), anti-CD21-FITC (1:300, BD Pharmingen, 561769, RRID: AB_10924591), anti ICOS-FITC (1:200, 11-9949-82, RRID: AB_465458) and anti-IκNS (1:10, 4C1, HMGU). All antibodies are from eBiosciences except where indicated. For intracellular staining of FoxP3, cells were permeabilized and fixed (eBiosciences, 00-5223-56), washed once with permeabilization buffer (eBiosciences, 00-8333-56) and stained for 30 min with anti-FoxP3-

PE (1:100, eBiosciences, 12-5773-82, RRID: AB_465936) in permeabilization buffer. Cells were washed with sorting buffer and analyzed using an Attune Acoustic Focusing Cytometer (Thermo Fisher) or a Fortessa Cytometer (Becton Dickinson, Franklin Lakes, NJ). For intracellular IκBNS and extracellular ICOS staining see supplemental materials.

Cultivation, stimulation and inhibitor treatment of cell lines and primary cells

All cell lines were maintained in humidified atmosphere (37°C, 5% CO_2). Jurkat T cells were cultured in RPMI 1640 Medium and maintained at a density between 0.5x and 1.5x 10^6 cells/ml. HEK293T cells were kept in DMEM and diluted after treatment with 0.05% trypsin/EDTA solution when reached a confluency of more than 80%. Media were supplemented with 10% fetal calf serum, 100 U/ml penicillin and 100 µg/ml streptomycin (all Gibco). Jurkat T cells were verified by the Authentication Service of the Leibniz Institute (DSMZ). HEK293T cells were obtained by DSMZ (RRID: CVCL_0045/CVCL_0063) and verified by DSMZ. Primary murine splenocytes were isolated from spleen, treated with Red Blood Cell Lysis Solution (Miltenyi) and CD4 T cells purified by using the CD4 T cell isolation kit II (Miltenyi) by negative magnetic-activated cell sorting (MACS). CD4 T cells were cultured in primary T cell medium (RPMI 1640, 100 U/ml penicillin, 100 µg/ml streptomycin, 10% heat inactivated fetal calf serum, 10 mM HEPES pH 7.5, 2 mM L-Glutamine, 1 mM Sodium-Pyruvate, MEM-NEAA (1x), 50 nM β-Mercaptoethanol (all Gibco). Jurkat T cells were stimulated with Phorbol 12-Myristate 13-Acetate (PMA, 200 ng/ml; Merck)/Ionomycin (Iono, 300 ng/ml; Calbiochem), mouse anti-human CD3 (1µg/ml; BD Pharmingen #555336; RRID: AB_395742)/-CD28 (3.3µg/ml; BD Pharmingen #555725; RRID: AB_396068) in presence of rat anti-mouse IgG1 (1.65µg/ml; BD Pharmingen #553440; RRID: AB_394860) and IgG2a (1.65µg/ml; BD Pharmingen #553387; RRID: AB_394825) (all BD Pharmingen) or recombinant human TNFα (20 ng/ml, Biomol). CD4 T cells were stimulated with PMA (200 ng/ml)/Iono (300 ng/ml) or hamster anti-mouse CD3 (0.5 µg/ml; 145-2C11; BD Bioscience #557306; RRID: AB_396632)/-CD28 (1 µg/ml; 37.51; BD Bioscience #553295; RRID: AB_394764) on rabbit anti-hamster IgG (Jackson ImmunoResearch #307-005-003; RRID: AB_2339572) pre-coated plates. For *in vitro* treatment of Jurkat T cells with MLT-

943 (*28*) or MLT-985 (*37*), cells were seeded in 6-well plates and incubated with the respective inhibitor concentrations for 24 hours in humidified atmosphere, respectively.

Analyses of IκBNS and ICOS expression by flow cytometry

For intracellular IκBNS and extracellular ICOS staining, primary murine splenocytes ($1x10^6$) were collected, centrifuged (300 x g, 5 min, 4 °C) and washed twice with PBS. Afterwards, live/dead staining (Fixable Viability Dye eFluor 780, 1:1000 in PBS, eBioscience #65-0865-14) was added for 30 min at 4°C. Cells were washed again with PBS, fixed in 2 % PFA for 20 min at 4 °C and permeabilized in Saponin buffer (0,5 % saponin and 1% BSA in PBS) for 25 min at RT. Unspecific antibody binding was blocked with anti-CD16/32 (1:100 in Saponin buffer, 10 min, 4 °C, eBioscience #14-0161-81, RRID: AB_467132) before samples were incubated with anti-IκBNS antibody (clone 4C1, rat, 1:10 in Saponin buffer, HMGU core facility monoclonal antibodies, RRID: N/A) for 30 min at 4 °C. Cells were washed (300 x g, 5 min, 4 °C) and stained with a secondary mouse anti-rat-AF647 (1:200 in Saponin buffer, 30 min at 4 °C, Biolegend #405416, RRID: AB_2562967). In parallel, anti-ICOS-FITC antibody in Saponin buffer was added (eBiosciences #11-9949-82, RRID: AB_465458). Samples were again washed (300 x g, 5 min, 4 °C) and wells were filled up with Saponin buffer to wash out unbound antibodies (> 15 min, RT). For surface staining, anti-CD4-PerCP (eBiosciences #45-0042-82, RRID: AB_1107001) and anti-CD8-PE (BD Pharmingen #553033, RRID: AB_394571) was added for 30 min at RT. Samples were again washed with FCM buffer (300 x g, 5 min, 4 °C), re-suspended in FCM buffer and acquired on an Attune Cytometer.

Preparation of tissue sections and histopathological evaluation

Tissue from mice was fixed in 10% neutral buffered formalin, embedded in paraffin (both Thermo Fisher Scientific, Waltham, Massachusetts, United States of America), cut at 4 µm using a microtome (Leica Biosystems, Nussloch GmbH, Nussloch, Germany), mounted onto glass slides (Thermo Fisher Scientific) and stained by Hematoxylin and Eosin (Thermo Fisher Scientific) using standard protocols

on an automatic stainer (AutostainerXL, Leica Biosystems). Glass slides were scanned at 400x (AperioCS2, Leica Biosystems) and subsequently evaluated using an open source software for digital visualization and analysis (QuPath, v.0.2.3, University of Edinburgh, Scottland, United Kingdom) (*57*). Representative images were exported using the same software.

In vitro Treg cell suppression assay

Treg suppression assays were performed as described previously (*21*). CD4+CD25-CD45RB^{hi} conventional naive T cells and CD4+CD25+CD45RB^{lo} Treg cells were sorted with a FACS Aria III (BD Biosciences). Conventional CD4+ T cells were labeled with 10 µM Cell Proliferation Dye eFluor 450 (Thermo Fisher Scientific) according to the manufacturer's protocol. 2.5×10^4 labeled conventional naive CD4+ T cells were plated alone or in presence of varying numbers of Treg cells in RPMI-1640/10% FBS complete medium into a 96-well U-bottom plate. Following the addition of 1 µg mL^{-1} (final concentration) of soluble anti-CD3 clone 17A2 (eBioscience, 100201, RRID: AB_312658) and 5×10^4 splenocytes that had been irradiated with 30 Gy using a BIOBEAM 3000 gamma irradiation device, cells were incubated for 3 days at 37 °C and 5% CO_2. Subsequently, the cells were subjected to flow cytometric analysis on a FACSCanto II (BD Biosciences).

Preparation of cell lysates

For cellular analysis via WB, Jurkat or primary murine CD4 T cells (2-3x10^6) were washed 1x in PBS and lysed in co-immunoprecipitation (co-IP) buffer (25 mM HEPES pH 7.5, 150 mM NaCl, 0.2% NP-40, 10% glycerol, 1 mM DTT, 10 mM NaF, 8 mM β-glycerophosphate, 300 µM sodium vanadate and protease inhibitor cocktail mix (Roche)) for 20 min at 4°C. For cellular lysis of EMSA samples, a high salt buffer was used (20 mM HEPES pH 7.9, 350 mM NaCl, 20% glycerol, 1 mM $MgCl_2$, 0.5 mM EDTA, 0.1 mM EGTA, 1% NP-40, 1 mM DTT, 10 mM sodium fluoride, 8 mM β-glycerophosphate, 300 µM sodium vanadate and Roche protease inhibitor cocktail mix). Lysate controls were mixed with 4x SDS loading dye, boiled for five min at 95°C, separated by SDS-PAGE and analyzed by WB.

Western blotting (WB)

An electrophoretic semi-dry blotting system was used to transfer SDS-PAGE separated proteins onto PVDF-membranes (Merck Millipore). After transfer, membranes were blocked with 5% BSA (Sigma-Aldrich) or 5% milk (Roth) in PBS-Tween (0.01% Tween) for 1 hour at RT. Primary antibodies were diluted as indicated in 2.5% BSA or milk in PBS-T and membranes incubated overnight at 4°C. Membranes were washed 3x 15 min with PBS-T and treated with HRP-coupled secondary antibodies (1:7000 in 1.25% BSA or milk in PBS-T) for 1 hour at RT. HRP was detected by enhanced chemiluminescence using the LumiGlo reagent kit (Cell Signaling Technologies) according to the manufacturer's specifications and visualized on ECL Amersham Hyperfilms (GE Healthcare). Images were cropped for presentation. WB antibodies used: anti-CARD11 (1D12; #4435; RRID: AB_10694496), anti-IκBα (L35A5; #4814; RRID: AB_390781), anti-p-IκBα (Ser32/36, 5A5; #9246; RRID: AB_2151442), anti-p65 (D14E12; #8242; RRID: AB_10859369), anti-p-p65 (93H1; #3033; RRID: AB_331284), anti-E-tag (13419; #13419; RRID: AB_2798215), anti-p-Akt (#9271; RRID: AB_329825), anti-Akt (#9272; RRID: AB_329827) (all Cell Signaling Technology); anti-MALT1 (B-12 for human; #sc-46677; RRID: AB_627909) (D-1 for murine; #sc-515389; RRID: N/A), anti-β-Actin (C4, 1:20.000; #sc-47778; RRID: AB_2714189), anti-CYLD (E-10; #sc-74435; RRID: AB_1122022), anti-HOIL-1 (H-1; #sc-393754; RRID: N/A), anti-BCL10 (H-197; #sc-5611; RRID: AB_634292) (all Santa Cruz); anti-Regnase-1 (#MAB7875; RRID: N/A) (R&D); anti-TRAF6 (EP591Y; #ab33915; RRID: AB_778572) (Abcam); anti-Roquin-1/2 (clone 3F12, 1:10, HMGU core facility monoclonal antibodies); HRP-conjugated anti-rabbit (#711-035-152; RRID: AB_10015282), HRP-conjugated anti-mouse (#715-035-150; RRID: AB_2340770), HRP-conjugated anti-rat (#112-035-062; RRID: AB_2338133) (all Jackson ImmunoResearch, 1:7000); all antibodies were used at 1:1000 dilution if not otherwise stated.

Electrophoretic Mobility Shift Assay (EMSA)

EMSAs were carried out using double stranded NF-κB (H2K fwd: 5'-GATCCAGGGCTGGGGATTCCCCATCTCCACAGG-3', H2K rev: 5'-GATCCCTGTGGAGATGGGGAATCCCCAGCCCTG-3') and OCT1 (fwd: 5'-GATCTGTCGAATGCAAATCACTAGAA-3', rev: 5'-GATCTTCTAGTGATTTGCATTCGACA-3') binding sequences which were radioactively labeled with [α-^{32}P] dATP using Klenow Fragment (NEB). Whole cell lysates (6-10 µg) were incubated for 30 min with shift-buffer (20 mM HEPES pH 7.9, 120 mM KCl, 4% Ficoll, 5 mM DTT, 10 µg BSA and 2 µg poly-dI-dC (Roche)) and radioactively labelled double stranded probes (10.000-20.000 cpm). Samples were applied on a 5% polyacrylamide gel in TBE buffer, vacuum-dried and exposed to Amersham autoradiography films (GE Healthcare).

Image stream analysis

Splenocytes were isolated from control, Traf6-ΔT or TBM-T mice, and either left untreated or stimulated with PMA (200 ng/ml)/Iono (300 ng/ml) for 30 min at 37°C. Fc receptors were blocked with anti-CD16/32 clone 93 (1:200, 14-0161-81, eBioscience, RRID: AB_467132), and cells stained with anti-CD4-APC (1:200, L3T4, 17-0041-83, eBioscience, RRID: AB_469321) for 15' at 4°C. Upon fixation and permeabilization for 1 hour at RT using Foxp3/Transcription factor staining buffer set (00-5523-00, eBioscience) according to the manufacturer's protocol, cells were subjected to intracellular staining with anti-p65 (1:200, D14E12, Cell Signaling Technology #8242, RRID: AB_10859369) or anti-c-Rel (1:200, sc-71, Santa Cruz Biotechnology #sc-71, RRID: AB_2253705)) for 1 hour at 4°C. After staining with a fluorescein isothiocyanate-coupled anti-rabbit IgG secondary antibody (1:200, 554020, BD Pharmingen, RRID: AB_395212) for 30 min at 4°C, 2µg/ml 4′,6-diamidino-2-phenylindole (Thermo Fischer) were applied to stain cell nuclei. The stained cell suspensions were subjected to flow cytometric analysis on an ImageStreamX Mark II (Amnis Merck Millipore). Data were analyzed using the IDEAS software (Amnis Merck Millipore) in which nuclear translocation is determined by quantification of the correlation of nuclear stain and intensity of the translocation probe, yielding a similarity score. High similarity score (high correlation) represents strong nuclear

translocation, whereas low similarity scores indicate cytoplasmic localization. Histogram overlays were generated using FlowJO analysis software (BD).

Detection of active MALT1 by activity based probes (ABP)

Generation and application of biotin-labeled MALT1 activity based probes (MALT1-ABPs) has been described previously (*30*). Jurkat T cells ($3x10^7$) were washed with PBS and lysed in 600 µl co-IP buffer without protease inhibitors for 25 min at 4°C. Cleared lysates (>20.000 x g, 4°C, 10 min) were used to collect lysate control (60µl) or incubated with High Capacity Streptavidin Beads (Thermo Fisher, 12µl) for 1 hour at 4°C for pre-clearing (490µl). Beads were pelleted (1700 x g, 2 min, 4°C) and 420 µl of supernatant mixed with biotin-labeled MALT1-ABP at a final concentration of 0.1 µM. After 50 min rotating at RT, High Capacity Streptavidin Beads (Thermo Fisher, 15µl) were added and samples incubated for 1-2 hours at 4°C (rotating). Beads were collected (1700 x g, 2 min, 4°C), washed 3x with co-IP buffer without protease inhibitors, resuspended in 22 µl 2xSDS loading dye, boiled at 95°C for 7 min and analyzed by WB.

Analysis of MALT1A and MALT1B splice isoforms

RNA from $1x10^7$ purified CD4+ T cells were isolated by resuspending in 600 µl TRIzol and incubating 5 min at RT. 120 µl chloroform was added and samples were vortexed for 15 sec followed by 3 min incubation at RT. Samples were centrifuged at 13,000 rpm for 5 min at 4°C and the colorless upper aqueous phase was transferred to a new microtube. The same volume of 70% Ethanol was added and samples were resuspended. Further RNA purification was performed with the RNeasy Mini Kit (Qiagen) and RNA was reverse transcribed (Verso cDNA synthesis kit, Thermo Fisher). To determine endogenous MALT1 IsoA/B levels, semi-quantitative PCR with 15 ng cDNA was performed using Taq DNA Polymerase (NEB) with primers flanking exons 7 *(*ex6 fw: 5′-ACCGAGACAGTCAAGATAGC-3′; ex9/10 rev: 5′-GACTTTGTCCTTTGCCAAAGG-3′) and detecting both isoforms MALT1A (146 bp) and MALT1B (113 bp). Hydroxymethylbilane synthase (Hmbs) served as control (fw: 5′-

GCGCTAACTGGTCTGTAGGG-3′; rev: 5′-TGAGGGAAAGGCAGATATGGAGG-3). PCR products were analyzed using 3% agarose gels.

Supplementary Figures and Tables

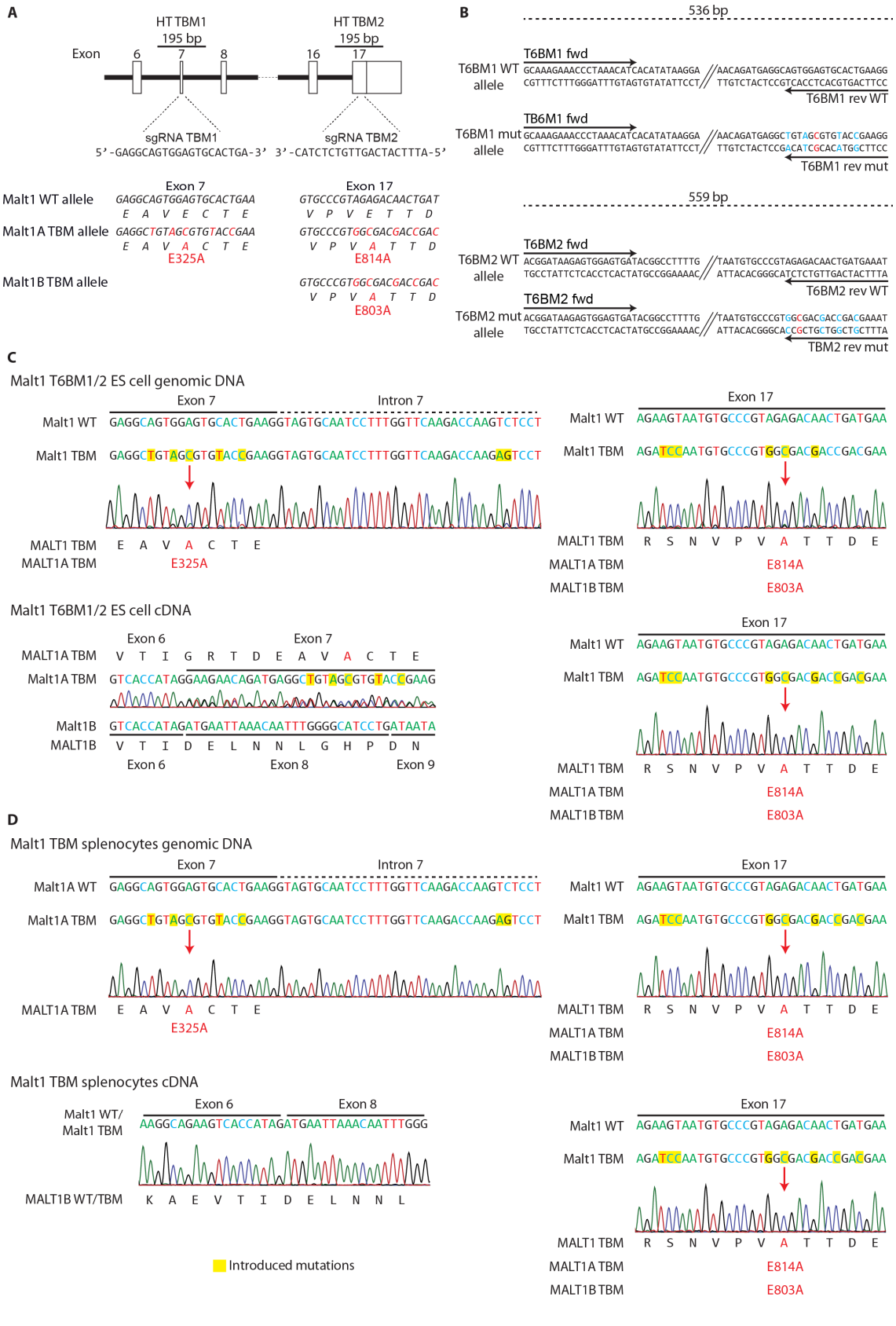

Fig. S1: Generation and verification of MALT1 TBM mutant embryonic stem (ES) cells and mice. (A) Schematic depiction of genomic organization of murine *Malt1* Exon 7 and Exon 17 encoding for T6BM1 and T6BM2, respectively. Single guide (sg) RNA sequences targeting T6BM1 and T6BM2 are shown. DNA and amino acid sequences for T6BM1 (Exon 7) and T6BM2 (Exon 17) regions are depicted. Below targeting strategy and alterations in the genomic DNA (including missense and silent mutations) is shown and translation to MALT1A E325A;E814A and MALT1B E803A protein expression. (B) Strategy for differential PCR genotyping of T6BM1 and T6BM2 wt and mutant alleles. (C and D) Sanger sequencing of genomic region and cDNA spanning T6BM1 (Exon 7) and T6BM2 (Exon 17) verifying the correct mutagenesis in *Malt1*$^{TBM/TBM}$ ES cells (C) and in *Malt1*$^{TBM/TBM}$ splenocytes (D). Genomic and cDNA sequencing verified correct mutations in T6BM1 and T6BM2. Note on cDNA sequences: *Malt1A* and *Malt1B* are expressed in ES cells leading to two overlapping ex6-ex7-ex8 and ex6-ex8 sequences. Correct mutations in Exon7 of *Malt1A* cDNA have been verified by sequence deconvolution. *Malt1A* mRNA is not expressed in splenocytes and only sequences for *Malt1B* cDNA lacking Exon7 are detected.

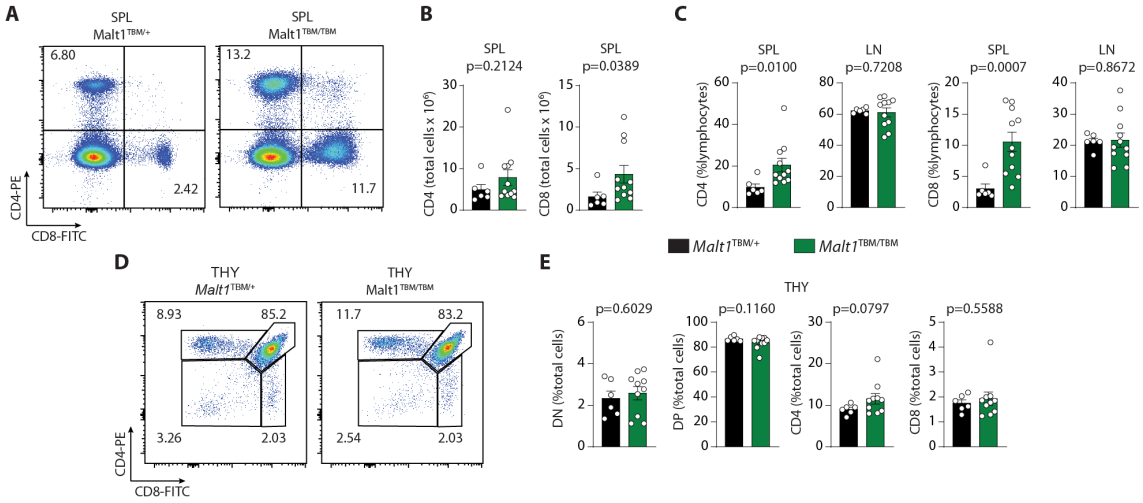

Fig. S2: Analysis of T cell numbers in *Malt1* TBM mice. (A to C) Flow cytometric analysis of CD4+ and CD8+ T cells (A) and quantifications showing total numbers (B) in spleen (SPL) or relative numbers (C) in SPL and lymph nodes (LN) in *Malt1*$^{TBM/+}$ and *Malt1*$^{TBM/TBM}$ mice. (D and E) Flow cytometric analysis of CD4+ and CD8+ double negative (DN), double positive (DP) or single positive thymic T cells (D) and quantification of relative numbers (E) of DN, DP and single positive CD4+ and CD8+ T cells from thymus of *Malt1*$^{TBM/+}$ and *Malt1*$^{TBM/TBM}$ mice. All analyses were performed with animals at day 18 after birth. Heterozygous *Malt1*$^{TBM/+}$ littermates (black) were compared to *Malt1*$^{TBM/TBM}$ mice (green). Each dot represents one mouse (six to eleven mice per group). All bars show the mean ± SEM and p-values were calculated by unpaired t-test with Welch's correction.

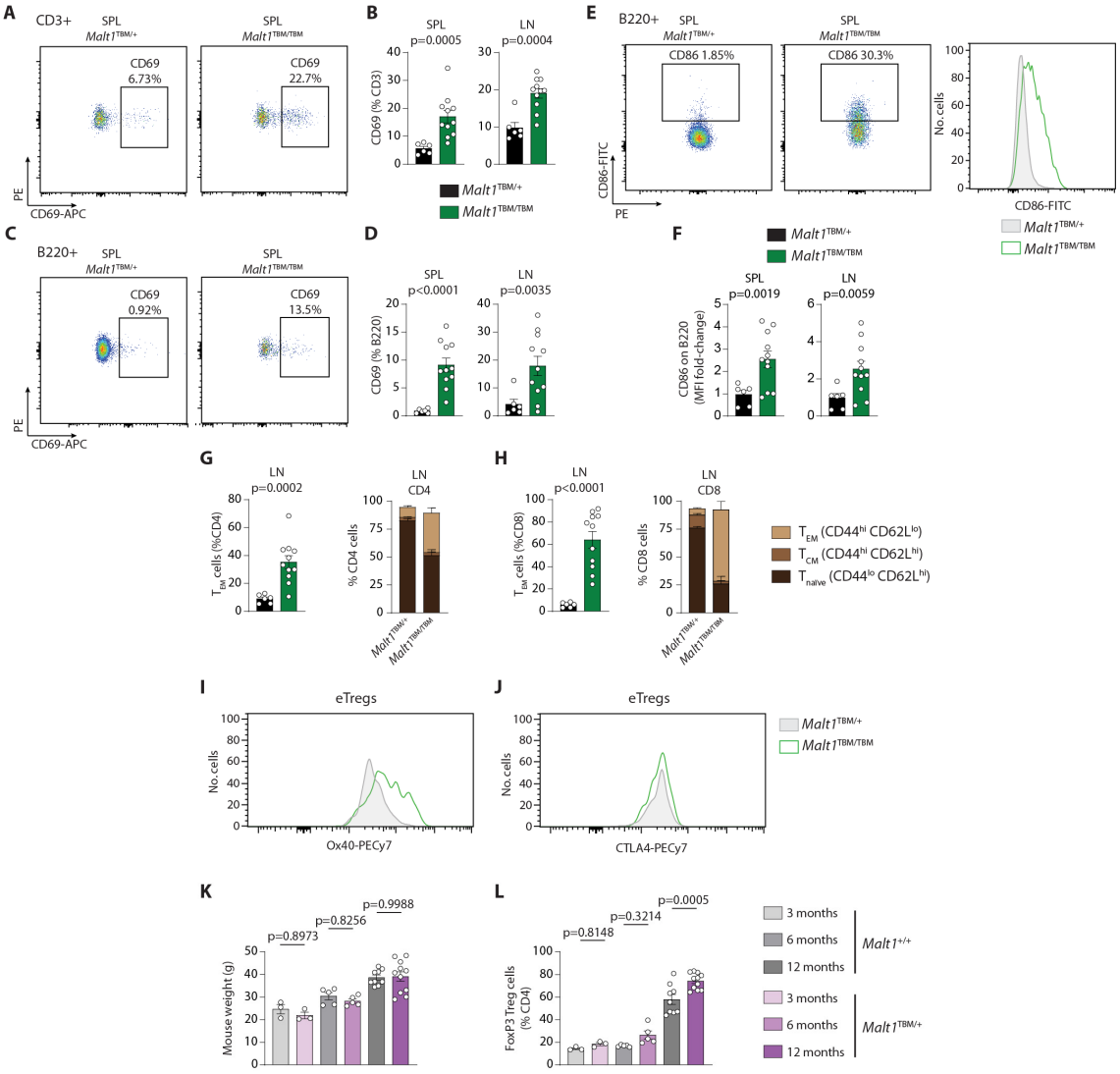

Fig. S3: Staining of lymphocyte activation and Treg cell markers in *Malt1* TBM mice. (A to D) Flow cytometric analysis of CD69+ staining on CD3+ (A) and B220+ (C) lymphocytes. Quantification of relative numbers of CD69+ CD3+ T (B) or B220+ B (D) cells from SPL and LN of *Malt1*$^{TBM/+}$ and *Malt1*$^{TBM/TBM}$ mice. (E and F) Flow cytometric analysis of CD86+ staining on B220+ lymphocytes (E) and fold change of CD86 mean fluorescence intensity (MFI) (F) on B220+ B cells from SPL and LN between *Malt1*$^{TBM/+}$ and *Malt1*$^{TBM/TBM}$ mice. (G and H) Quantifications of relative numbers of CD44^{hi}CD62L^{lo} T_{EM} cells (left) and relative numbers of $T_{naïve}$ (CD44^{lo}CD62L^{hi}), T_{CM} (CD44^{hi}CD62L^{hi}) and T_{EM} CD4+ (G) and CD8+ (H) T cells from lymph nodes (LN) of *Malt1*$^{TBM/+}$ and *Malt1*$^{TBM/TBM}$ mice. (I and J) Representative histograms for OX40 (I) and CTLA-4 (J) staining on CD44^{hi}CD62L^{lo} effector eTreg cells from spleen of *Malt1*$^{TBM/+}$ and *Malt1*$^{TBM/TBM}$ mice. (K) Mouse weights of *Malt1*$^{+/+}$ and *Malt1*$^{TBM/+}$ mice at an age of 3, 6 or 12 months. (L) Relative numbers of CD4+FoxP3+ Treg cells in SPL of *Malt1*$^{+/+}$ and *Malt1*$^{TBM/+}$ mice at an age of 3, 6 or 12 months. All analyses (except K and L) were performed with animals at day 18 after birth and heterozygous *Malt1*$^{TBM/+}$ littermates (black) were compared to *Malt1*$^{TBM/TBM}$ mice (green). Each dot represents one mouse (B-H: six to eleven mice per group, K, L: three to eleven mice per group). All bars show the mean ± SEM and p-values were calculated by unpaired t-test with Welch's correction (in B, D, F, G and H) or by ordinary one-way analysis of variance (ANOVA) combined with Tukey's multiple comparisons test (K and L).

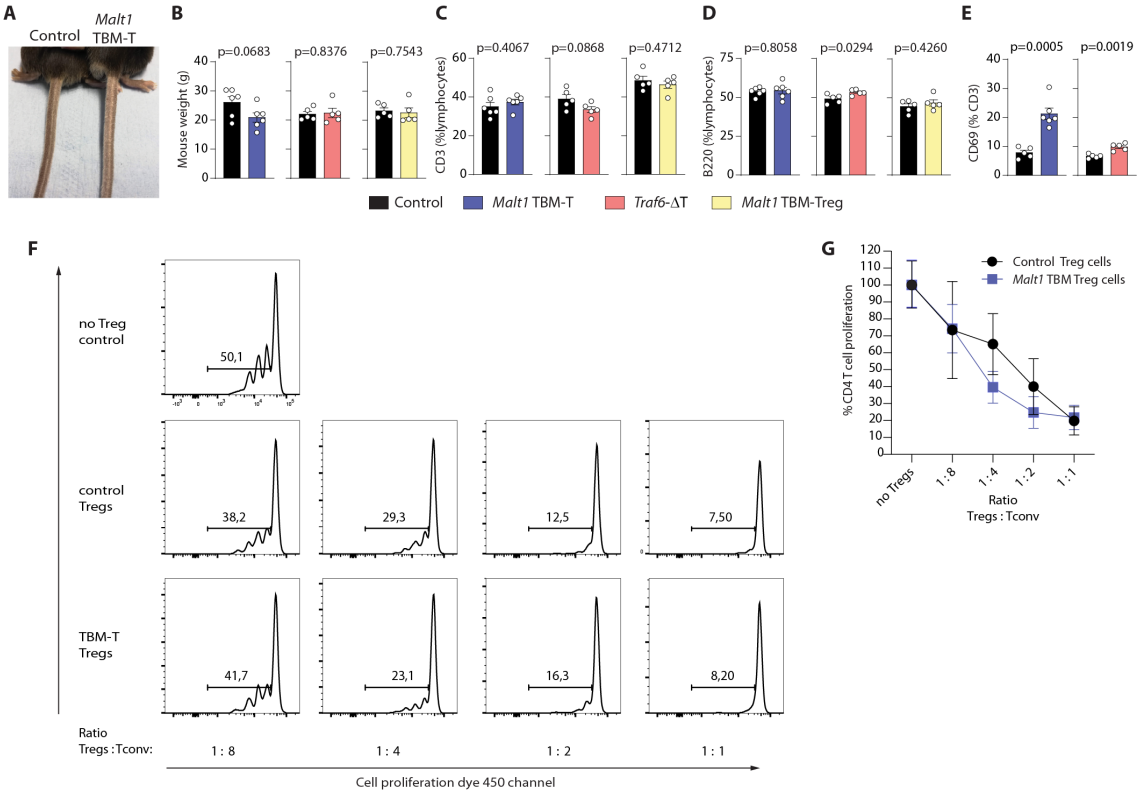

Fig. S4: Phenotypic analysis of *Malt1* TBM-T, *Traf6*-ΔT and *Malt1* TBM-Treg mice. (A) Picture of mouse tails showing skin eczema in *Malt1* TBM-T versus control mice. (B) Mouse weights of control, *Malt*1 TBM-T, *Traf6*-ΔT and *Malt*1 TBM-Treg mice. (C and D) Relative numbers of CD3+ T (C) and B220+ B (D) cells in control, *Malt*1 TBM-T, *Traf6*-ΔT and *Malt*1 TBM-Treg mice. (E) Relative numbers of CD69+ CD3+ T cells from control, *Malt*1 TBM-T, *Traf6*-ΔT and *Malt*1 TBM-Treg mice. (F) *In vitro* Treg-suppressor assays showing representative FACS plots of proliferation dye 450 labelled conventional CD4+ T cells (Tconv) cultivated without (no Tregs) or with increasing numbers of Treg cells (ratio 1:8 to 1:1) of control or *Malt1* TBM-T mice in the presence of irradiated splenocytes and αCD3. (G) Suppression of conventional CD4+ T cell proliferation by control and *Malt1* TBM Treg cells (see F) was quantified by determining the percentage of CD4+ T cells displaying dye 450 dilution compared to control (no Treg cells). Data were normalized to the mean Tconv proliferation in the absence of Treg cells (no Tregs) and show the mean ± SD from three biological replicates. Two-way ANOVA with Sidak's multiple comparison correction was performed ($p>0.11$ for all ratios). All immune cell stains were performed with splenic cells. Littermate control mice were $Malt1^{fl/+}$*;CD4-Cre-*, $Malt1^{fl/+}$;CD4-Cre+ and $Malt1^{TBM/fl}$*;CD4-Cre-* or $Traf6^{fl/+}$*;CD4-Cre+*, $Traf6^{fl/fl}$*;CD4-Cre-* and $Traf6^{fl/+}$*;CD4-Cre- or* $Malt1^{fl/+}$*;FoxP3-Cre-*, $Malt1^{fl/+}$;FoxP3-Cre+ and $Malt1^{TBM/fl}$*;FoxP3-Cre-* (black) for *Malt1* TBM-T (blue) or *Traf6*-ΔT (rose) or *Malt1* TBM-Treg (yellow), respectively. Each dot in panels B-E represents one mouse (five to six mice per group). Treg suppression assay was performed with 3 sets of mice (control and TBM-T). All bars (B-E) show the mean ± SEM and p-values were calculated by unpaired t-test with Welch's correction.

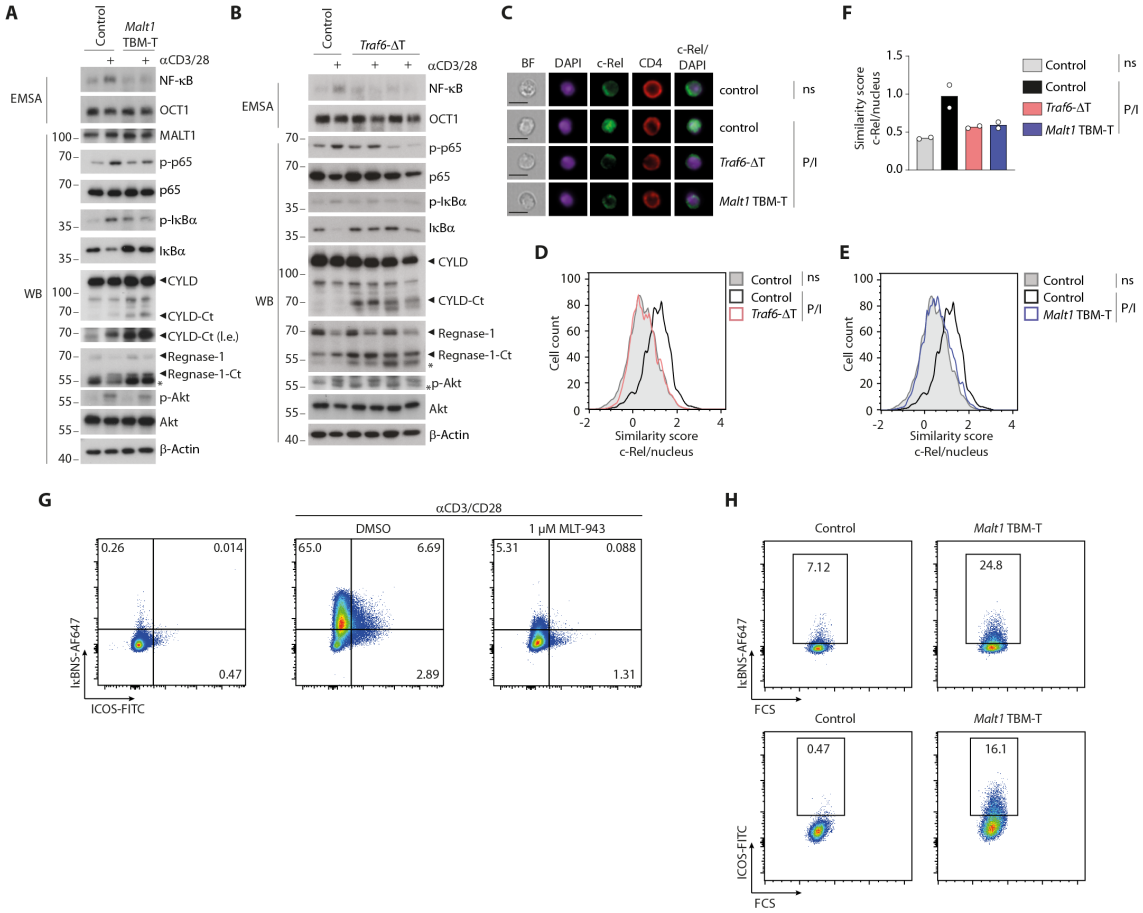

Fig. S5: Defective NF-κB and chronic MALT1 protease activation in *Malt1* TBM-T and *Traf6*-ΔT mice. (A and B) Analyses of NF-κB DNA binding (EMSA), canonical NF-κB signaling and MALT1 substrate cleavage (WB) after αCD3/CD28 stimulation of splenic CD4+ T cells from control, *Malt1* TBM-T (A) and *Traf6*-ΔT (B) mice. Asterisks indicate unspecific signals. (C to F) Image stream analysis showing representative pictures (BF: bright field; scale bars: 10 μm) (C), histograms showing similarity scores of c-Rel and DAPI stain (D and E) and quantification of c-Rel and DAPI similarity scores from two independent experiments (F) in splenic CD4+ T cells of control, *Malt1* TBM-T and *Traf6*-ΔT mice after P/I stimulation. (G) Flow cytometric analysis of IκBNS and ICOS positive CD4+ T cells after 5h stimulation with αCD3/CD28 antibodies and co-treatment with the MALT1 inhibitor MLT-943 (1 μM). (H) Flow cytometric analysis of IκBNS and ICOS expression on CD4+ T cells from spleen of control and *Malt1* TBM-T mice. All analyses were done with mice at 8-12 weeks of age. Littermate control mice were *Malt1*$^{fl/+}$*;CD4-Cre-, Malt1*$^{fl/+}$;CD4-Cre+ and *Malt1*$^{TBM/fl}$*;CD4-Cre-* or *Traf6*$^{fl/+}$*;CD4-Cre+,Traf6*$^{fl/fl}$*;CD4-Cre-* and *Traf6*$^{fl/+}$*;CD4-Cre-* (black) for *Malt1* TBM-T (blue) or *Traf6*-ΔT (rose), respectively.

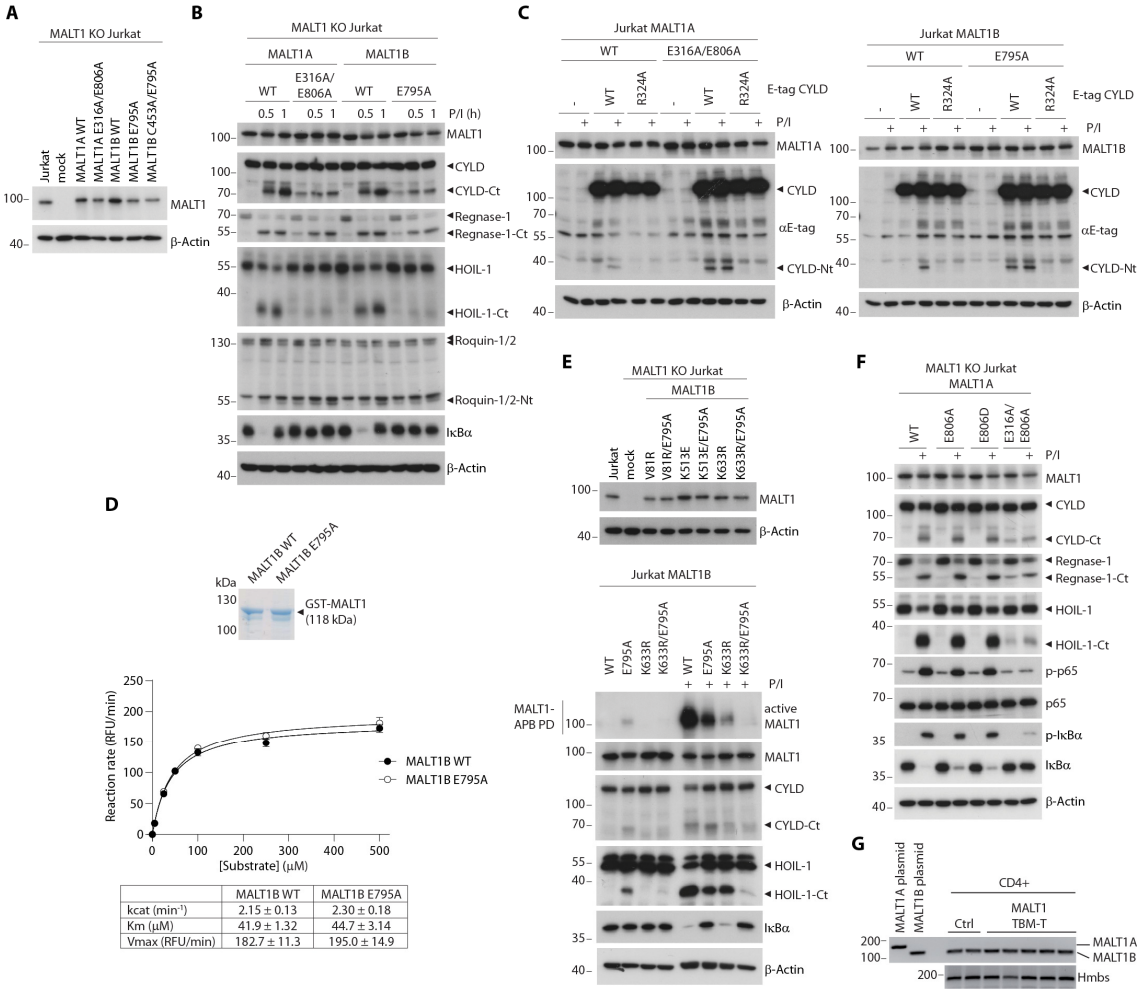

	MALT1B WT	MALT1B E795A
kcat (min^{-1})	2.15 ± 0.13	2.30 ± 0.18
Km (μM)	41.9 ± 1.32	44.7 ± 3.14
Vmax (RFU/min)	182.7 ± 11.3	195.0 ± 14.9

Fig. S6: NF-κB activation and MALT1 protease activity upon loss of TRAF6-MALT1 interaction in Jurkat T cells. (A and B) Expression of MALT1 WT and mutant constructs (A) after reconstitution of MALT1 KO Jurkat T cells and analyses of MALT1 substrate cleavage and IκBα degradation (B) after reconstitution with MALT1A and MALT1B WT or T6BM mutants MALT1A E316A/E806A and MALT1B E795A untreated or stimulated with P/I by WB. (C) Transfection of E-tagged CYLD WT or the MALT1 cleavage insensitive mutant R324A in MALT1A WT or MALT1A E316A/E806A (left) and MALT1B WT or MALT1B E795A expressing (right) Jurkat T cells. Constitutive and P/I-inducible (60 min) cleavage of E-tagged CYLD was assessed by WB. (D) Coomassie gel of purified recombinant GST-MALTB WT and GST-MALT1B E795A (upper panel) and measurement of Michaelis-Menten kinetics by increasing the concentration of Ac-LRSR-AMC substrate was used to calculate kcat, Km and Vmax. Graph and values depict the mean ± SEM from three independent experiments. (E) Expression analyses of MALT1 WT and mutant constructs (upper panel) after lentiviral reconstitution of MALT1 KO Jurkat T cells and analyses of MALT1 activity by biotin-MALT1-ABP assay and substrate cleavage (lower panel) after reconstitution with MALT1B WT and mutants alone or in combination with the T6BM mutant (E795A) of untreated or P/I stimulated (60 min) cells by WB. (F) MALT1 KO Jurkat cells were reconstituted with patient-derived MALT1A E806D variant. Cells were left untreated or stimulated with P/I (30 min) and NF-κB signaling and MALT1 substrate cleavage was determined in WB. (G) Analysis of *Malt1A* and *Malt1B* mRNA expression by RT–PCR in CD4+ T cells from *Malt1*$^{TBM/+}$ (control) and *Malt1*$^{TBM/TBM}$ mice. Migration of amplified *Malt1A* and *Malt1B* plasmid controls is shown and hydroxymethylbilane synthase (HMBS) mRNA served as internal control.

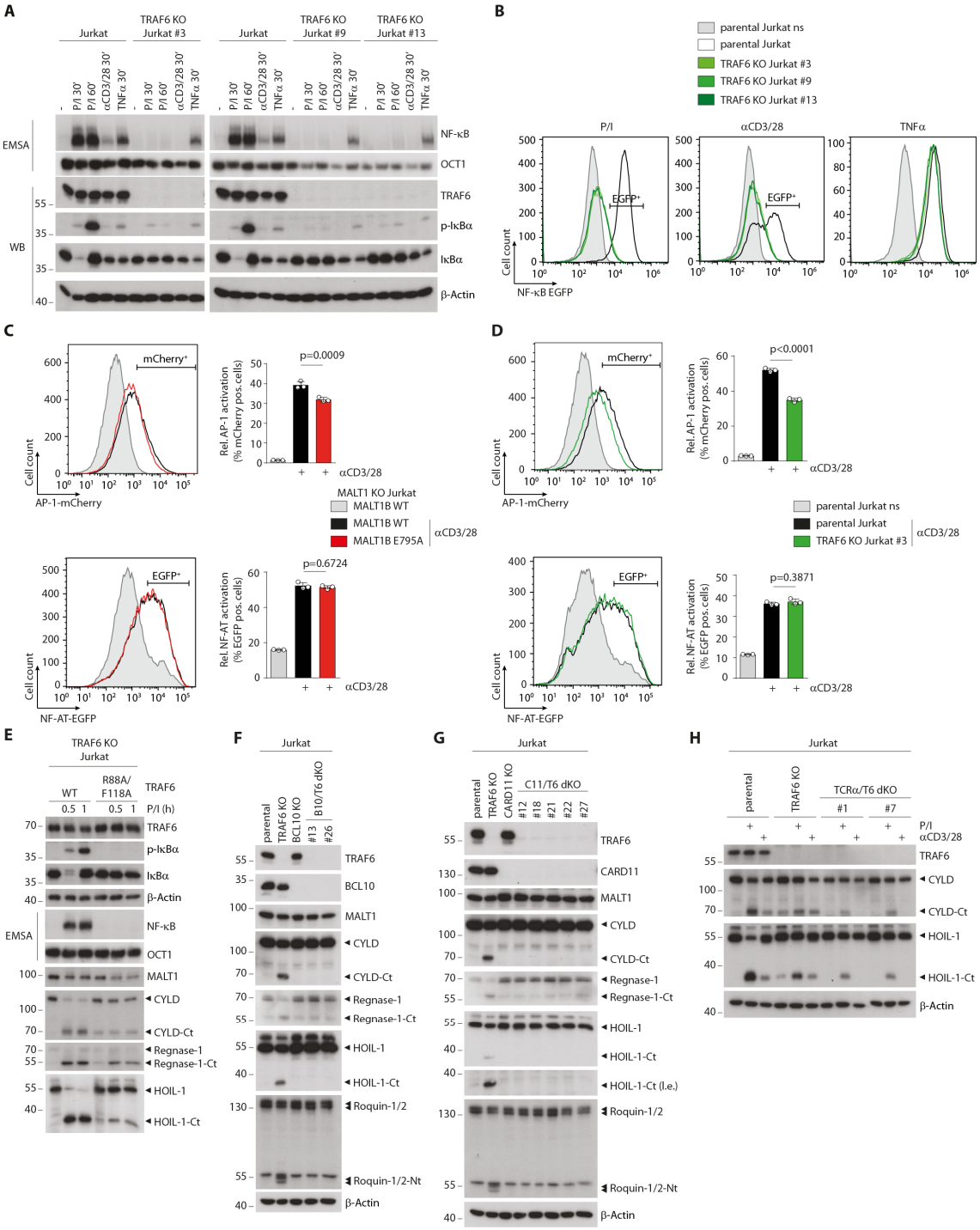

Fig. S7: NF-κB activation and MALT1 protease activity upon ablation of TRAF6 in Jurkat T cells. (A) Parental and TRAF6 KO Jurkat T cells were stimulated with P/I, αCD3/28 or TNFα. NF-κB signaling and activation was determined by WB and EMSA. (B) Parental and TRAF6 KO Jurkat T cells transduced with an NF-κB-EGFP reporter were stimulated with αCD3/28, P/I or TNFα and NF-κB activation was assessed by flow cytometry of EGFP positive cells. (C and D) MALT1B WT or E795A reconstituted Jurkat T cells (C) or TRAF6 KO Jurkat T cells (D) transduced with an AP-1-mCherry or NF-AT -EGFP reporter genes were stimulated with αCD3/28 and NF-κB activation was assessed by flow cytometry of fluorescence positive cells. Bars show quantification of fluorescence positive cells from three independent experiments including the mean ± SEM and p-values were calculated by

ordinary one-way analysis of variance (ANOVA) combined with Dunnett's multiple comparisons (E) TRAF6 KO Jurkat T cells reconstituted with TRAF6 WT or mutant R88A/F118A were analyzed for NF-κB signaling (WB and EMSA) and MALT1 substrate cleavage (WB) with and without P/I stimulation. (F and G) Parental, TRAF6 KO and different TRAF6/BCL10 (F) and TRAF6/CARD11 (G) dKO Jurkat T cells were analyzed for constitutive MALT1 substrate cleavage by WB. (H) Parental, TRAF6 KO and TRAF6/TCRα dKO Jurkat T cells were analyzed for constitutive and inducible MALT1 substrate cleavage after αCD3/CD28 or P/I stimulation (60 min) by WB.

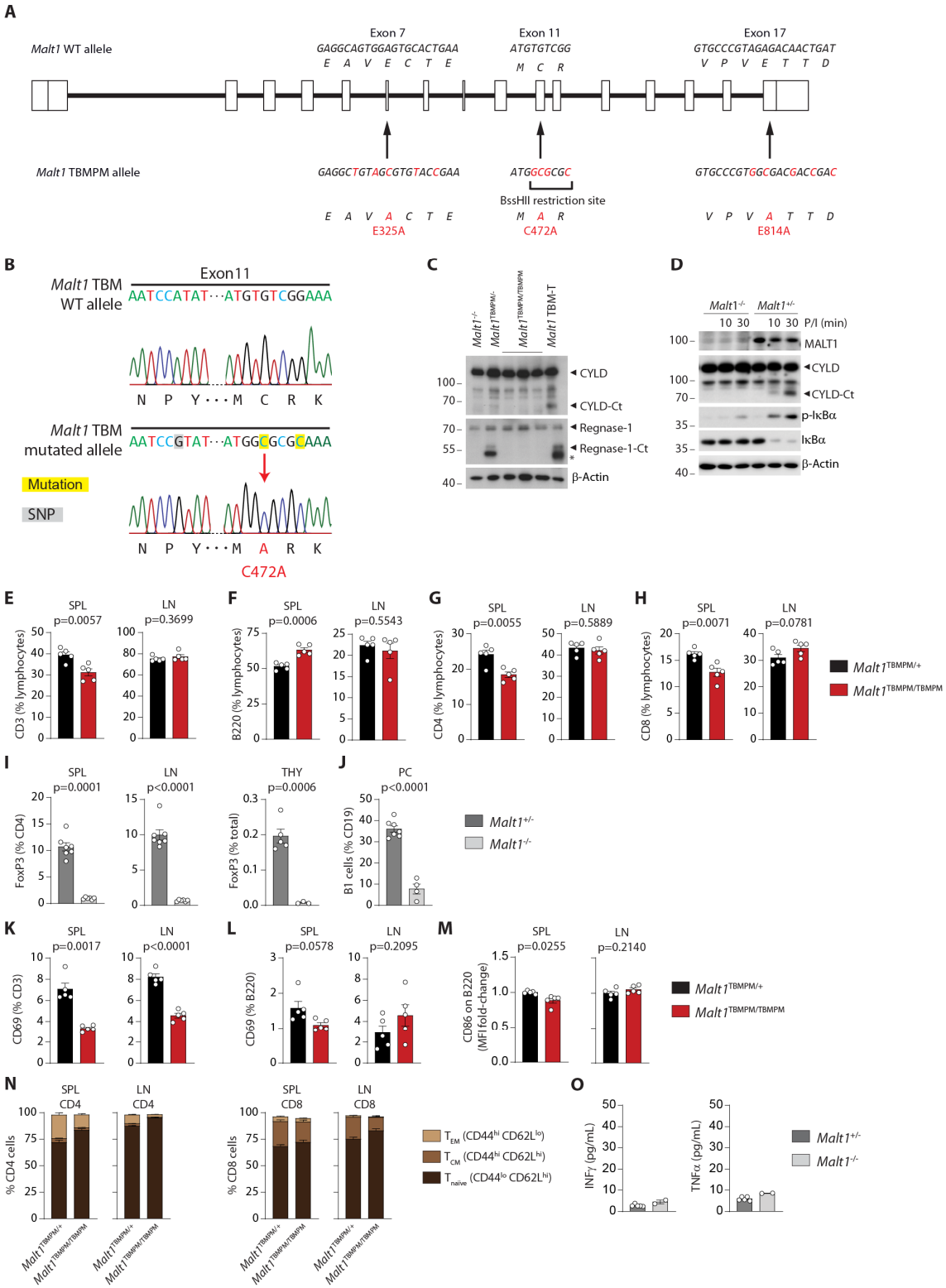

Fig. S8: Generation and analyses of *Malt1* TBMPM mice. (A) Schematic depiction of genomic organization of murine *Malt1* locus and sequences in Exon 11 that were altered to mutate C472A (PM) in the *Malt1* TBM allele carrying the TBM1 (E325A) and TBM2 (E814A) mutations. (B) Sequencing of genomic region in exon 11 indicating paracaspase mutation C472A and the ES cell-derived silent SNP c.1323A/c.1323G serving as a marker for the *Malt1* TBM allele. (C) MALT1 substrate cleavage in isolated splenic CD4+ T cells from Malt1$^{-/-}$, *Malt1*$^{TBMPM/+}$, *Malt1*$^{TBMPM/TBMPM}$ and *Malt1*$^{TBM/fl}$;CD4-

Cre+ (Malt1 TBM-T) mice. (D) IκBα phosphorylation and degradation and CYLD cleavage in splenic CD4+ T cells isolated from *Malt1*$^{-/-}$ and *Malt1*$^{+/+}$ mice. (E to H) Relative numbers of CD3+ (E) T cells, B220+ (F) B cells, CD4+ (G) T cells and CD8+ (H) T cells from SPL and LN of *Malt1*$^{TBMPM/+}$ and *Malt1*$^{TBMPM/TBMPM}$ mice. (I and J) Relative numbers of CD4+Foxp3+ Treg cells from SPL, LN and thymus (I) and B1 cells from peritoneal cavity (J) of *Malt1*$^{+/-}$ and *Malt1*$^{+/+}$ mice. (K and L) Relative numbers of CD3+CD69+ T (K) or B220+CD69+ (L) B cells from SLP and LN of *Malt1*$^{TBMPM/+}$ and *Malt1*$^{TBMPM/TBMPM}$ mice. (M) Fold change of CD86 MFI on B220+ B cells from SPL and LN between *Malt1*$^{TBMPM/+}$ and *Malt1*$^{TBMPM/TBMPM}$ mice. (N) Relative numbers of $T_{naïve}$, T_{CM} and T_{EM} CD4+ and CD8+ T cells from SPL and LN of *Malt1*$^{TBMPM/+}$ and *Malt1*$^{TBMPM/TBMPM}$ mice. (O) Concentrations of IFNγ and TNFα in sera of *Malt1*$^{+/-}$ and *Malt1*$^{-/-}$ mice. All analyses were performed with animals 8 weeks after birth. Each dot represents one mouse (E-N: three to seven mice per group). All bars show the mean ± SEM and p-values were calculated by unpaired t-test with Welch's correction.

Table S1: CRISPR guides and homology templates.

Description	Name	DNA sequence
CRIPSR-Cas9 targeting of Malt1 (murine)	T6BM1 sgRNA	5’-GAGGCAGTGGAGTGCACTGA-3’
	T6BM2 sgRNA	5’-ATTTCATCAGTTGTCTCTAC-3’
	PM sgRNA	5’-TGTTCCTGTTGGATATGTGT-3’
	T6BM1 ssODN HDR	5’-TCTCTGTTGACTTAATGACTACCCTTCCTAAGA TATGAGTTACAATATGTTCACATTTGTTTTCTCTA AATAAGGAAGAACAGATGAGGCTGTAGCGTGTA CCGAGGTAGTGCAATCCTTTGGTTCAAGACCAAG AGTCCTCATGCTGCATGCTGGTTACTCTGGGGAG AGGTGGAGGTCCTAGCTCACT-3’
	T6BM2 ssODN HDR	5’-CCAGACAGGTGTCATTGCAGCCGGACTCCACA CACATTCATTTCAAATTATCCCCCCCACCACTACT GCCAGTTTGGTAGATCCAATGTGCCCGTGGCGA CGACCGACGAAATGCCATTCAGTTTTTCTGACAG GCTTATGATTTCTGAAAACTGACCTTCATGGTTTT GAAAATTAGAATAGTTACAGTAATCT-3’
	PM ssODN HDR	5’-CCTGTTGATGCTCCAAATCCATATAGGTCTGA AAATTGCCTATGCGTACAAAACATACTGAAATTA ATGCAAGAAAAGGAGACTGGCCTGAATGTGTTC CTGTTGGATATGGCGCGCAAAAGGTAAAATGTC TCATCTCTCTATCAAGTAGCAACCTTGACAAAGT CTATGTAAGGCAATTCTGTACGGTGGTAA-3’
CRISPR-Cas9 targeting of Traf6 (Jurkat)	Traf6 exon1 sgRNA	5’-TGTTACAGCGCTACAGGAGC-3’
	Traf6 exon2 sgRNA	5’-ATGGTGAAATGTCCAAATGA-3’
CRISPR-Cas9 targeting of TCRα (Jurkat)	TCRα exon 1 sgRNA	5’-ACAAAACTGTGCTAGACATG-3’

Table S2: Genotyping primers.

Description	Name	DNA sequence
Malt1 TBM1 genotyping	T6BM1 fwd general	5'-GCAAAGAAACCCTAAACATC-3'
	T6BM1 rev WT-specific	5'-CCTTCAGTGCACTCCACT-3'
	T6BM1 rev Mut-specific	5'-CCTTCGGTACACGCTACA-3'
Malt1 TBM2 genotyping	T6BM2 fwd general	5'-ACGGATAAGAGTGGAGTGAT-3'
	T6BM2 rev WT-specific	5'-ATTTCATCAGTTGTCTCT-3'
	T6BM2 rev Mut-specific	5'-ATTTCGTCGGTCGTCGCC-3'
Malt1 knockout genotyping	Malt1 flox del fwd	5'-CTAGTCAGTCACCAGCTCAG-3'
	Malt1 flox del rev	5'-CTGGCTAACCAATCCTCAAAAC-3'
	Malt1 flox rev	5'-CAGTTCTCAATGCCAACGCAC-3'
FoxP3-Cre genotyping	FoxP3-Cre TG fwd	5'-CGGGTCAGAAAGAATGGTGT-3'
	FoxP3-Cre TG rev	5'-CAGTTTCAGTCCCCATCCTC-3'
	FoxP3-Cre ctrl fwd	5'-CAAATGTTGCTTGTCTGGTG-3'
	FoxP3-Cre ctrl rev	5'-GTCAGTCGAGTGCACAGTTT-3'
CD4-Cre genotyping	CD4-Cre fwd	5'-ACCAGCCAGCTATCAACTCG-3'
	CD4-Cre rev	5'-TTACATTGGTCCAGCCACC-3'
Traf6 genotyping	Traf6 fwd	5'-CATGGCTTGTTACCTCTGCTC-3'
	Traf6 wt/flox rev	5'-TCCAGCAGTATTTCATTGTCAAC-3'